Microfluidic Serologic Assay for Point of Care Detection

by

Kylie Snow

A Thesis Presented in Partial Fulfillment
of the Requirements for the Degree
Master of Science

Approved April 2022 by the
Graduate Supervisory Committee:

Karen Anderson, Chair
Jennifer Blain Christen
Douglas Lake

ARIZONA STATE UNIVERSITY

May 2022

ABSTRACT

Human papillomavirus (HPV) infection has a large burden on society. It is a causal agent of 99.7% of all cervical cancer cases. The prevalence of HPV infection worldwide is high, but the burden of HPV infections lies on less developed regions. Cervical cancer is not associated with immediate symptoms, screening methods are needed to detect HPV disease presence before lesions progress to cervical cancer. Protein biomarkers are a growing area of diagnostic medicine and facilitate the detection of disease at an early and treatable stage. Technologies for healthcare diagnostics often require laboratory space or expensive instrumentation, which are not feasible for point of care applications. In order for clinical diagnostics to advance in developing countries, low cost, rapid, portable, and easy to use point of care diagnostic tests are needed.

The project adapts the Enzyme Linked Immunosorbent Assays (ELISA) and Nucleic Acid-Programmable Protein Array (NAPPA) to a proof of concept assay for use in magnetic bead based microfluidics. The biomarker used for analyte detection was E7, as a strong correlation has been found between presence of E7 antibodies and development of advanced cervical cancer. It is demonstrated that magnetic microfluidic assay design for rapid detection of antibodies is amenable to fluorescence detection in point of care settings. The data demonstrates that the microfluidic assay is rapid, low-cost, specific, and relevant to serology detection. The assay detects antibody responses to analytes with the point of care reader system and is realized in an on chip capacity. With the integration of anti-GST capture antibodies conjugated to the magnetic beads in the microfluidic system, many analytes can be detected without large changes to the existing assay structure, which gives the ability to adapt the system to analytes of interest rapidly.

ACKNOWLEDGMENTS

I would like to thank Dr. Karen Anderson and the members of my committee for their support and guidance over the course of this project. I would also like to thank Marika Hopper for her mentorship on diagnostic assay design and development, Siril Arockiam for his advice on experimentation, Vi Nguyen for her assistance in the creation of the microfluidic chip, and Joshua Eger for his help in utilizing the point of care reader.

TABLE OF CONTENTS

Page

LIST OF TABLES

LIST OF FIGURES

Figure Page

Figure Page

CHAPTER 1

INTRODUCTION

HPV Infection Life Cycle

Human papillomaviruses (HPVs) are non-enveloped, double stranded, DNA viruses. There are more than 200 different HPV types, and HPV induced pathologies range from benign warts to malignant cancers depending on the strain and site of infection (Smola, 2017). HPV enters the cells of the basal layer of the epithelium, likely requiring mild abrasion or microtraumas in the epidermis to gain entry into the cells (Burd, 2003). Upon entry the HPV virus can evade immunity for many months, due to its infectious cycle. With initial HPV infection very little viral proteins are expressed and viral replication occurs in cells already destined for natural cell death, or death by anoikis. In this way there is no inflammatory response and no alert to the immune system (Stanley, 2010). HPV viruses are separated into low, intermediate, and high-risk categories, depending on their association with cancer (Bergot et al., 2011). HPV can infect both cutaneous and mucosal surfaces. Cutaneous types of HPV infect the hands and the feet, and mucosal types of HPV infect the lining of the mouth, throat, and respiratory tract, as well as the anogenital epithelium (Burd, 2003). HPV types 6, 11, 40, 42, 43, 44, and 54 are examples of low risk types, and cause benign warts. HPV types 16, 18, 31, 33, 35, 39, 45, 51, 52, and 58 are examples of high risk types, they infect mucosal surfaces and are oncogenic (Bergot et al., 2011; Braaten & Laufer, 2008). HPV 16 is the most oncogenic strain, it is found in nearly 90% of the noncervical cancers associated with HPV as well as roughly half of all cervical cancer cases, and HPV 16 and HPV 18 together are detected in 70% of cervical cancer cases (Jemal et al., 2013; Braaten &

Laufer, 2008). HPV infection develops into cervical cancer during a progression from precancerous lesions called CIN1, CIN2, and CIN3 to cancer. This process is not immediate and takes years or decades to occur (Smola, 2017). Most HPV infections clear within one to two years and even most HPV induced lesions regress spontaneously within one year, but in some cases they can persist for five years or more and develop the histological markings of CIN1 lesions (Bergot et al., 2011). Seventy percent of women with HPV infections became negative within one year and ninety one percent became negative within 2 years, though some strains of HPV are more likely to cause persistence. HPV 16 for example had a 2 year clearance rate of seventy two percent (Braaten &Laufer, 2008). If precancerous CIN1 lesions develop, they can progress further to CIN2 and CIN3, with 1% developing into cancer, or they can regress, with sixty percent of CIN1 lesions regressing spontaneously. If lesions progress to CIN3, the regression rate lessens to approximately thirty three percent, and the likelihood of progression into cervical cancer rises to twelve percent (Braaten & Laufer, 2008). When cancer develops HPV DNA has been found to be mostly integrated into the cellular genome of infected cells, and this integration of the HPV genome into the host cell genome is considered to be a crucial event in tumor development and progression (Bergot et al., 2011; De Freitas et al., 2014). The HPV genome encodes for two structural proteins, Late 1 (L1) and L2, and six nonstructural proteins, Early 1 (E1), E2, E4, E5, E6, and E7. Early proteins control DNA replication within the infected cells by altering the cell cycle and promoting the replication of the viral genome. Late proteins form the capsid and pack the virion (Bergot et al., 2011). The viral proteins E6 and E7 are recognized as the universal oncogenic drivers of cancers associated with HPVs and their persistent expression is

necessary for this transition (Munger et al., 2013). Integration of the HPV genome into the host cell genome causes cleavage at the site of the E1/E2 genes, which deletes the E2 gene and regions adjacent of the E4, E5, or L2 genes. E2 is a DNA binding protein that blocks transcription of E6 and E7 (De Freitas et al., 2014). E6 and E7 function to subvert cell growth regulatory pathways and facilitate viral replication in cells that are terminally differentiated and have exited the cell cycle. When E2 blocks the transcription of E6 and E7 this permits E1 to bind to viral origin of replication and initiates replication of the viral genome in the S phase of the cell cycle, which allows for a constant level of genome copy number and low level of expressed transcripts. Since the E2 gene is responsible for downregulating the E6 and E7 genes, when it becomes cleaved during genome integration, E6 and E7 become overexpressed (Burd, 2003) HPV E6 and E7 essentially function to reprogram host cell signaling transduction pathways, inserting additions to signaling that are nonessential and redundant in normal cells (Munger et al., 2013). E6 and E7 are able to immortalize human keratinocytes and extend the lifespan of infected cells, as well as suppress the interferon response by inhibiting the interferon signaling pathway and effectively delaying the activation of adaptive immunity (Abdulkarim et al., 2002; Stanley, 2010). The E6 and E7 proteins also neutralize the function of tumor suppressor proteins P53 and pRb (Abdulkarim et al., 2002). The proteins P53 and pRb serve to regulate the cell cycle and maintain the integrity of the cellular genome, and in most cancers these proteins are mutated. The HPV proteins E6 and E7 do not mutate these proteins in cervical cancer development, rather they bind to the wild type conformations of the protein and neutralize their activity in that way, and E6 and E7 proteins from high risk HPVs especially have high binding affinity for these proteins

(Abdulkarim et al., 2002; Burd, 2003). E6 oncoprotein binds to P53 and uses the ubiquitin proteolytic pathway to promote its degradation and inhibit its growth function. E7 oncoprotein targets hypophosphorylated pRb for ubiquitin mediated proteolysis. These low levels of p53 and pRb lead to aberrant cell cycle checkpoint control and high rates of mutagenesis (Abdulkarim et al., 2002). E6 and E7 of high risk HPVs are so effective at blocking these negative regulator proteins that the consistent cell cycle progression causes cells to have genomic instability and accumulate genetic alterations that drive the malignant transformation (Crosbie et al., 2013).

Burden of HPV Infection

HPV infection has a large burden on society, it is a causal agent of 99.7% of all cervical cancer cases, 90% of anal cancer cases, more than 60% of subsites of oropharyngeal cancer cases, and 40% of vaginal, vulvar, and penile cancer cases (Jamal et al., 2013). The World Health Organization reported that approximately 12% of all cancer cases globally are cervical cancer cases making it the most common gynecological malignancy in the world (Dasari et al., 2015). The strains HPV 16 and HPV 18 are the cause of 70% of cervical cancer cases worldwide with type 16 detected in 24% of women with HPV infection and type 18 detected in 9% with HPV infection worldwide (Jamal et al., 2013; Crosbie et al., 2013). HPV is highly prevalent and is the most common sexually transmitted infection, for example, in the United States 80% of women acquire it before the age of 50. While the prevalence of HPV infection worldwide is high, the burden of HPV infections lies mostly on the less developed regions of the world due to financial, logistical, and sociocultural constraints to screening and prevention (Braaten &Laufer, 2008; Black & Richmond, 2018). Cervical cancer is the fifth most common cancer

among humans, the second most common cancer among women worldwide, and is the most common cancer mortality cause among women in developing countries (Kaarthigeyan, 2012; Vinodihini et al., 2012). Roughly nine out of ten cervical cancer deaths occur in less developed regions, with 1/5th of the world burden of cervical cancer deaths occurring in Africa, and 1/5th of the world burden of cervical cancer deaths occurring in India alone (Ngoma & Autier, 2019; Sankaranarayanan et al., 2019). In India, 98% of the oncogenic HPV strains circulating are HPV 16 and HPV 18 with HPV 16 having 80 to 90% prevalence (Bharadwaj et al., 2009). These strains are found in 80 to 85% of cervical cancer cases in India, which is more than the world average of 70% (Sankaranarayanan et al., 2019; Jamal et al., 2013). Additionally, the methods of screening and prevention that are well established in western counties are difficult to implement in low resource settings (Harries et al., 2009). Cervical cancer cases can be prevented with HPV vaccination and regular and timely cancer screening, but the access and use of HPV vaccines is limited in developing countries due to the cost of the vaccines (Van Dyne et al., 2018; Bergot et al., 2011). Pap smears, combined with treatment in the precancerous or early cancer stages, have resulted in the prevention of up to 80% of invasive cervical cancer cases in high resource settings, but many developing countries do not have screening programs, and those that do often have very low coverage due to lack of awareness, inadequate access, exam discomfort, or fear of finding cancer (Black & Richmond, 2018; Rositch et al., 2012). In the United States, there is an overall cervical cancer screening rate of 83% (Center for Disease Control and Prevention, 2012). In India, a study done by Montgomery et al. in 2015 found that 46% of women were accepting of vaccination in India, but only 21% were willing to have a pap smear. This is problematic

because early screening is important for positive health outcomes, especially in the absence of vaccination, and more than 75% of cervical cancer cases in India are diagnosed at a clinically advanced stage that gives patients poor prospects of survival (Sankaranarayanan et al., 2019).

HPV Biomarkers

Cervical cancer is not associated with immediate symptoms as other genitourinary pathologies are, therefore, it is important to have established screening methods to detect HPV disease presence before lesions progress from precancerous cells to invasive cervical cancer (Dasari et al., 2015). The slow progression of CIN1, CIN2, and CIN3 lesions from early cervical atypia to invasive cancer gives an opportunity to identify disease at a precancerous stage and begin treatments, as the prognosis of asymptomatic invasive disease is very poor but treatment of the preinvasive lesions is very effective (Dasari et al., 2015). Biomarkers are found in the blood, saliva, or other bodily fluids and provide a sign of abnormal conditions. A biomarker can be used to determine risk in cancer development and to detect changes in the early stages of disease, where patients can more effectively be treated. Protein biomarkers are a growing area of diagnostic medicine and facilitate the detection of disease at an early and treatable stage (Dasari et al., 2015). The biomarker chosen for this study was E7, as approximately 50% of patients with cervical cancer have humoral immune responses to the HPV E2, E6, and E7 oncoproteins, and a strong correlation has been found between presence of E7 antibodies and development of advanced cervical cancer (Reuschenbach et al., 2008; Bergot et al., 2011). Testing for HPV biomarkers is advantageous for many reasons. When atypical or borderline cytology is found in pap smear testing, about 60% of women test positive for

high risk HPV types. This additional testing along with cytology testing allows women who are negative for HPV to be routinely recalled at standard screening intervals whereas those who test positive for HPV can be referred to colposcopy. The immediate action for those most at risk and routine action for those who test negative for HPV reduces the stress caused by uncertainty and repeated examinations (Crosbie et al., 2013). In randomized trials in Europe and Canada, testing for HPV along with cytology resulted in greater detection of disease in the first screening round compared to cytology alone, and in India, screening based on testing for HPV presence along with cytology resulted in the reduction in the incidence of advanced cervical cancer cases and death compared with cytology or visual detection with acetic acid (Crosbie et al., 2013). Additionally, HPV testing in countries without effective cervical cancer cytology screening can be a simple strategy for population screening. Point of care HPV testing where regular cytology screening is not available could allow for women who test positive to be given further testing and treatment (Crosbie et al., 2013).

Existing Assays

There are two systems of serological assay that this project intends to adapt to the microfluidic platform, ELISA (Enzyme Linked Immunosorbent Assay) and NAPPA (Nucleic Acid-Programmable Protein Array). There are four types of ELISA, of which this project focuses on two of them, indirect ELISA and sandwich ELISA. An indirect ELISA utilizes a primary and secondary antibody for detection of an immobilized analyte. The primary antibody binds to the analyte and the secondary antibody is labeled with the molecule used for detection and binds to the primary antibody. The advantages of an indirect ELISA approach are high signal amplification and high flexibility due to

the ability of one or multiple secondary antibodies to bind a primary antibody and the ability of one secondary antibody to bind multiple types of primary antibodies (Cusabio Technology, 2018). For example, an anti-human IgG secondary antibody will bind any human IgG no matter what analyte that primary antibody can bind to. The disadvantage of an indirect ELISA approach is possible cross reactivity of the secondary antibody (Cusabio Technology, 2018). It is important to account for this in determining the background signal of the assay.

A sandwich ELISA utilizes a capture antibody, primary antibody, and a secondary antibody. In the sandwich ELISA the capture antibody is immobilized, and an analyte is added that the capture antibody then binds to and captures. The primary antibody binds to the analyte and the secondary antibody is labeled with the molecule used for detection and binds to the primary antibody. The advantages of a sandwich ELISA approach are high flexibility due to the ability to have a capture antibody that can capture multiple analytes and high specificity since it is necessary for two antibodies to bind to the analyte of interest. The disadvantage of a sandwich ELISA approach is that the analyte must be able to have the capacity for two antibodies to bind to it at different epitopes (Cusabio Technology, 2018). The capture antibody and the primary antibody must be able to bind the analyte in order for the assay to generate a signal, and if either one fails to bind then the assay will fail. This project utilizes the high flexibility of the sandwich ELISA for a point of care capacity. The capture antibody used in this project is the anti-GST antibody which can capture any protein with a GST tag. This approach is preferable over the indirect ELISA due to the ability to utilize a universal capture antibody during assay

construction. As long as the analytes of interest are expressed with GST tags, there is no need to create separate assays for each analyte of interest as in the indirect ELISA.

NAPPA is a method of conducting biological assays using protein encoded plasmid DNA. Proteins are generated from the plasmid DNA in situ using a cell free expression system (Miersch & LaBaer, 2011). NAPPA can be adapted to many biological assays, though this project utilized NAPPA in a sandwich ELISA immunoprecipitation assay. The advantages of NAPPA are that this approach circumvents challenges in protein purification and stability through the in situ expression with HeLa lysate (ASU Biodesign Institute, 2015). Cell free expression systems, also called In Vitro Transcription/Translation (IVTT), are often used when the desired analyte biomarkers are difficult to express proteins. IVTT is not limited to any host cell constraints such as homeostasis or viability (Jensen et al., 2021). This system is beneficial when using HPV protein biomarkers, such as E2 and E4, as they are very difficult to express recombinantly in bacterial systems. Adapting NAPPA to a sandwich ELISA immunoprecipitation assay increases the amount of analytes that can be targeted in a diagnostic point of care assay.

The ability to do routine assessments of biomarkers and serology in communities is beneficial for many areas of medicine, including clinical trials, diagnostics, and treatments of complex disease (Sorger, 2008). Technologies used for healthcare diagnostics often require laboratory space or expensive instrumentation, neither of which is feasible for remote locations or developing nations. In order for clinical diagnostics to advance in developing countries or areas without the appropriate infrastructure, low cost, rapid, portable, and easy to use point of care diagnostic tests are needed (Sonker et al., 2017). Existing commercial approaches for protein or biomarker assays are reliable in

laboratory settings but are not well adapted for point of care settings (Rusling et al., 2010). The traditional plate based ELISA is a very laborious and time consuming process, and alternative methods for simple, rapid, and sensitive biomarker detection is necessary (Tsai et al., 2019). Point of care diagnostic devices have many advantages in biomarker based diagnostics, such as rapid response and detection time, portability, lower cost, and no need for specialized laboratory equipment (Pandey et al., 2017). Most point of care assays utilize lateral flow assay formats (Lee et al., 2019). A lateral flow approach has multiple advantages, it can be used for quantitative or qualitative approaches, it has a long shelf life with no need for refrigeration, it can be made in large batches, and it has a low cost. The disadvantages of a lateral flow method are saturation of the nitrocellulose membranes which leads to a restriction on total volume, the analysis of samples is dependent on their viscosity, and the pores in the lateral flow can become clogged leading to leaking from the nitrocellulose membrane (Koczula & Gallotta, 2016). Lateral flow assays have known challenges in sensitivity and reproducibility, especially with serological testing and plasma. Sensitivity varies between antigens and certain antigens are difficult to utilize in a lateral flow capacity as they do not reach acceptable levels of sensitivity (Hou et al., 2018). Point of care diagnostic assays must follow the ASSURED methodology, i.e., they are Affordable, Sensitive, Specific, User-Friendly, Robust, Rapid, Equipment-free, and Deliverable. With lateral flow assays, as sensitivity increases typically so do costs and assay complexity (Zhu et al., 2017). Additionally, traditional lateral flows face challenges in multiplexing. Typically, a lateral flow strip will have one analyte of interest and then a positive or negative control or both (Koczula & Gallotta, 2016). The most common detection method for lateral flow assays is the use of a gold

conjugate as a reporter molecule, which results in visible bands for positive readings. If done in a qualitative capacity, visual reading of bands may be subjective and could lead to false positive or false negative interpretations. Lateral flow assays are limited to qualitative or semi-quantitative results (Lee et al., 2019).

The project adapts the existing indirect ELISA, sandwich ELISA, and NAPPA assays to applications on magnetic bead based microfluidics. The microfluidic applications were chosen due to the advantages of microfluidics in sensitivity and ease of application, which is an important aspect of point of care assay applications. Microfluidic applications integrated with biosensor technologies are likely to result in improved point of care diagnostics (Pandey et al., 2017). Current micro-fabrication technologies allow for microfluidics devices to have many compositions depending on the chemistries required for the assay. Microfluidic devices can be made out of glass, silicon, elastomers, plastics, paper, and more. The most common materials used to create microfluidic point of care assays are glass and plastics, though glass is falling out of favor due to its brittleness, cost, and lack of flexibility (Pandey et al., 2017). This project utilizes plastics as the base for the microfluidic device. Microfluidics can be used to create rapid, efficient, low cost, and portable diagnostic assays for use in limited resource settings or developing nations, and analysis of biomarkers is one of the most pursued applications for microfluidics assays (Sonker et al., 2017). There are several advantages to using microfluidic chips in point of care applications. Microfluidic chips can be integrated readily with multiple types of sensors, and they can process samples using very small quantities of reagents, additionally, they have the ability to store reagents dry on the chip, through lyophilization or conjugate pads, which makes for easier transport and storage of

the assays. On chip separation of plasma from blood is also possible through a mechanical filter on chip that holds back the larger red blood cells and matrix components but allows the plasma to pass through into the microfluidic channels. This removes the need for prior centrifugation or laboratory processing of samples and laborious benchtop practices. The ability to filter samples simplifies the analysis, and decreases analysis times (Sorger, 2008; Sonker et al., 2017). Antibody based microfluidic capture offers high selectivity and specificity towards antigens, but there must be modifications made to the device surface or a solid support incorporated into the microfluidic device to hold the antibodies or antigens and allow for this type of selective capture. Typically, microfluidic systems that are based on antibody capture use porous polymer monoliths, beads, or nanoparticles secured in the microchannels or wells in order to stabilize antibodies or antigens (Sonker et al., 2017). This project utilizes magnetic beads as a support for antigen and antibody based capture. Magnetic immunoassays have become useful for a variety of biochemical applications, as they allow for rapid separation and selective detection. The incorporation of magnetics in a microfluidic system has the potential to create a simple, rapid, and sensitive assay for detecting biomarkers (Tsai et al., 2019). Microfluidics are commonly adapted to laser induced fluorescence detection. Fluorescence detection is highly sensitive and selective and is beneficial for use in assays with low detection limits, such as biomarker assays (Tsai et al., 2019). Fluorescence detection is the optical detection method used in this project, and Quantum Dots were chosen for their superior brightness and narrow fields of excitation and emission as well as Alexa Fluor for their intense fluorescence and resistance to self-quenching.

Aims

It is important to develop an assay that can be used for non-invasive detection of cervical cancer biomarkers. Advances in microfluidic technology has given the ability of serology to move away from lateral flow. The overarching aim of this project is to develop a cost effective microfluidic based serologic assay that can detect immune response to analytes by using fluorescence detection in clinical settings. A secondary aim was to utilize In Vitro Transcription and Translation to develop an assay that can incorporate detection of weak analytes or analytes that are difficult to synthesize using traditional E. coli protein expression methods, creating a programmable detection assay. It was hypothesized that by utilizing magnetic beads in a microfluidic system it would enable decreased costs associated with serologic assays and increased sensitivity to analytes.

CHAPTER 2

MATERIALS AND METHODS

Point of Care Fluorescent Reader for Fluorescence Detection

Detection Methods and Reader Output

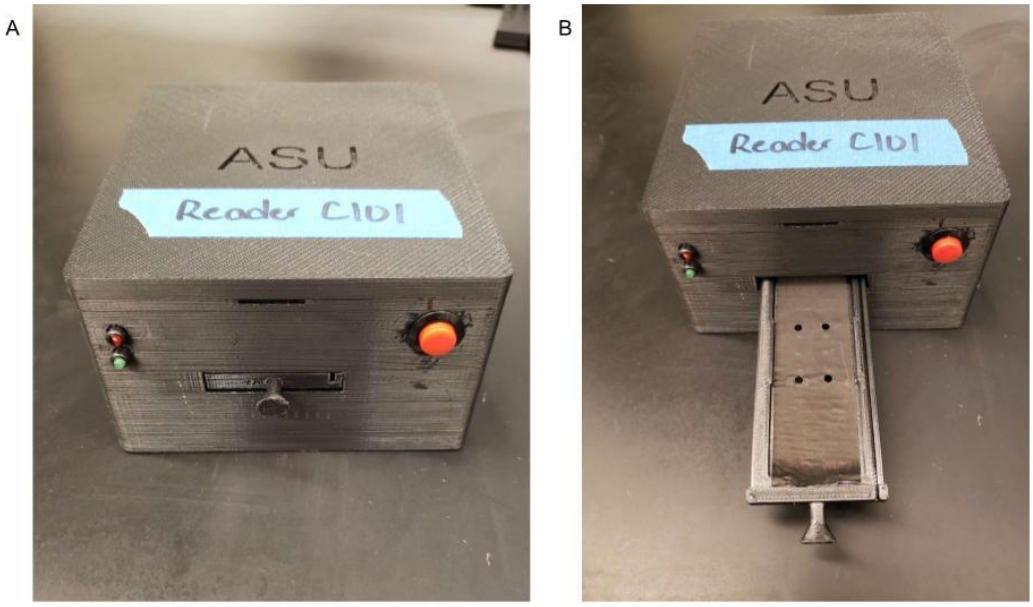

Figure 1: (A) The point of care reader. (B) The point of care reader cartridge for reading of the microfluidic chip. The point of care reader measures 121.5 mm long, 106.57 mm wide, and 58 mm high. The tray cutout is 38 mm wide, and 8 mm high.

There were two detection methods used in this study, a fluorescence detecting 96 well plate reader and a fluorescence detecting point of care reader (POC reader) engineered by the Blain Christen laboratory, which is reported in Obahiagbon et al., 2018. The plate reader is a SpectraMax M5 model and was used for laboratory verification of experiments. The point of care reader was used for verification that the assay can be performed in clinical applications, as the plate reader is cost prohibitive in point of care applications and non-portable while the point of care reader has been developed to be portable and cost effective (Obahiagbon et al., 2018). The point of care reader has been adapted from as described in Obahiagbon et al., 2018 to utilize different

excitation and emission filters to fit the microfluidic application and use of Q-dot 655 and Alexa Fluor 488. The output from each reader was analyzed and used to determine positivity or negativity of samples. The plate reader gives an output in fluorescence units. The brighter the fluorescence units the stronger the signal. The point of care reader gives an output of current measured in nanoamps. The higher the current the stronger the signal. Both outputs can be used to generate a signal to noise ratio, which is the ratio of the sample value divided by the negative control value in order to account for background or noise in the assay signal (Starcevic Manning et al., 2017). The signal to noise ratio is used to determine sample positivity to antigens, with a value higher than 2 indicating sample positivity stronger than background noise.

Microfluidic Chips

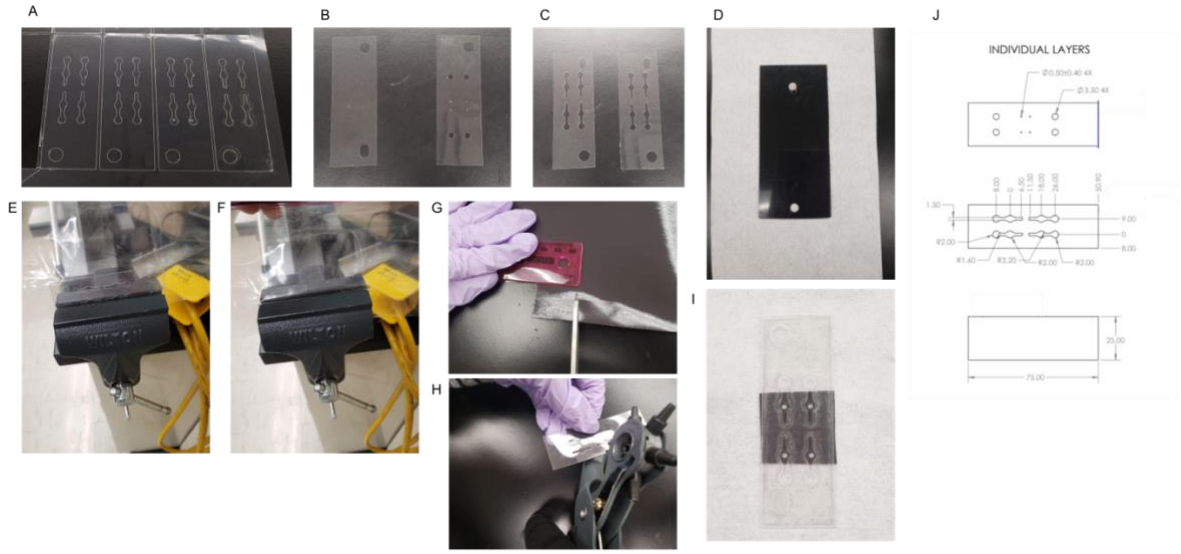

Figure 2: Construction of the microfluidic Chip (A) Pressure sensitive adhesive used in microfluidic chip construction. (B) Top and bottom layers of the microfluidic chip. (C) Inner layers of the microfluidic chip that give well structure. (D) Assembly block for the microfluidic chips to ensure even and consistent placement. (E) The microfluidic chip is placed in a plastic bag and air pockets are removed by hand press. (F) The microfluidic chip in the hand press. (G) The magnetic aperture described in the Magnetics section of the Materials is cut by hand to be a 1 inch by 1 inch square. (H) The 3 mm aperture holes described in the Magnetic Apertures section of the Materials are pressed out with a hand-held hole punch, a spare microfluidic layer is used as a template. (I) The final microfluidic chip design. (J) The dimensions of the microfluidic chip, in mm, adapted from a figure by Clifford Anderson of the Blain Christen lab.

The microfluidic chips that are used for the microfluidics are designed in collaboration with Dr. Blain Christen's lab and made on the Cricut Machine. The chips are made of 5, 7, or 9 layers depending on desired well capacity and utilize a combination of plastic types. The well capacity of the 5 layer chip is 17 uL, the well capacity of the 7 layer chip is 25 uL, and the well capacity of the 9 layer chip is 33 uL. Initial designs for the chips are created in SolidWorks, which are then uploaded into the Cricut software. The Cricut machine cuts the uploaded design into the plastics, which can then be assembled by hand. The final design chosen was the 7 layer microfluidic chip. The initial layer of the chip is a backing layer, it is made of polyethylene terephthalate 3 mils in size. The second, fourth, and sixth layers are an adhesive layer made of pressure sensitive adhesive. The third and fifth layer are the layers that establish the structure of the microfluidic wells and are made of polyethylene terephthalate 7 mils in size. The top layer is a protective layer which covers the well and establishes the input and output valves, it is made from polyethylene terephthalate 3 mils in size. Once assembled, the microfluidic chips are pressed in a manual hand press to flatten and remove imperfections. The microfluidic chips have four sample wells for a multiplexed design as well as an initial loading valve and an air exit valve. The microfluidic chips were used for magnetics and flow experiments.

The microfluidic chips were chosen due to their cost effectiveness, ease of construction, and flexibility for adaptations. The pressure sensitive adhesive used in the construction of the microfluidic chips does have levels of autofluorescence, that depend on the amount of adhesive used during construction and the amount of the adhesive that is exposed in the outer edges of the wells due to natural variance when constructing the

chips by hand. The microfluidic chips are compatible with multiple fluidics systems beyond the serology applications of this project.

Fluorophore Detection

Q-dot 655. The fluorophore used in this study was the Quantum Dot 655 (Q-dot 655) fluorophore *c*onjugated to an anti-mouse IgG or an anti-human IgG. The Q-dot was chosen for its superior qualities relative to traditional organic fluorescent dyes. The Q-dot is made of nanometer sized crystals from semiconductor materials. It has a broad excitation spectra and a narrow and symmetrical emission spectra as well as large Stokes shifts which allow for higher accuracy in quantification without inter-channel bleed throughs (Prost et al., 2016). The Q-dot also has high fluorescence efficiency, i.e., high molar extinction coefficients and quantum yields as high as 90%, which provides fluorescence outputs that surpass conventional dyes many times over. Additionally, the Q-dot photostability is about 1000-fold that of organic fluorescent dyes (Prost et al., 2016). Brightness and stability were the main factors evaluated when choosing the fluorescent dye to be used. While there are Q-dots in many wavelengths, Q-dot 655 was chosen as it is the brightest of the Q-dot wavelength offerings (Boston University, 2013).

Alexa Fluor 488. An additional fluorophore used in this study was the Alexa Fluor 488 fluorophore conjugated to an anti-mouse IgG or an anti-human IgG. The Alexa Fluor was chosen after experimental approaches indicated the need to diversify fluorophore scope used in the study. Alexa Fluor fluorophores are sulfonated rhodamine derivatives, and they exhibit a variety of characteristics that make them superior to spectrally similar fluorophores. Alexa Fluor fluorophores exhibit higher quantum yields which emits a more intense fluorescence, they have enhanced photostability, and pH

insensitivity, as well as a high degree of water solubility (Fish & Davidson, 2009). A characteristic of interest to this study is the ability of Alexa Fluor fluorophores to attach to proteins at high molar ratios, which enables brighter conjugates and no significant self-quenching (Thermo Fisher Scientific, 2015a).

Assay Adapting ELISA to Microfluidics

Indirect ELISA Proof of Concept

In order to adapt the indirect ELISA assay to microfluidics, MyOne Carboxylic Acid Dynabeads were conjugated to recombinant E7 protein in accordance with the protocol found in the product manual from Invitrogen Life Technologies. For proof of concept experiments anti-E7 mouse monoclonal was used to replicate the primary antibody and anti-mouse Fab2' antibody conjugated to Q-dot 655 was used as the secondary antibody. The primary was used at a 200 ng/mL concentration and the secondary was used at a concentration of 1:500 where 1 uL of the antibody was added to 499 uL of 1x phosphate buffered saline with 0.1% tween and 0.1% BSA.

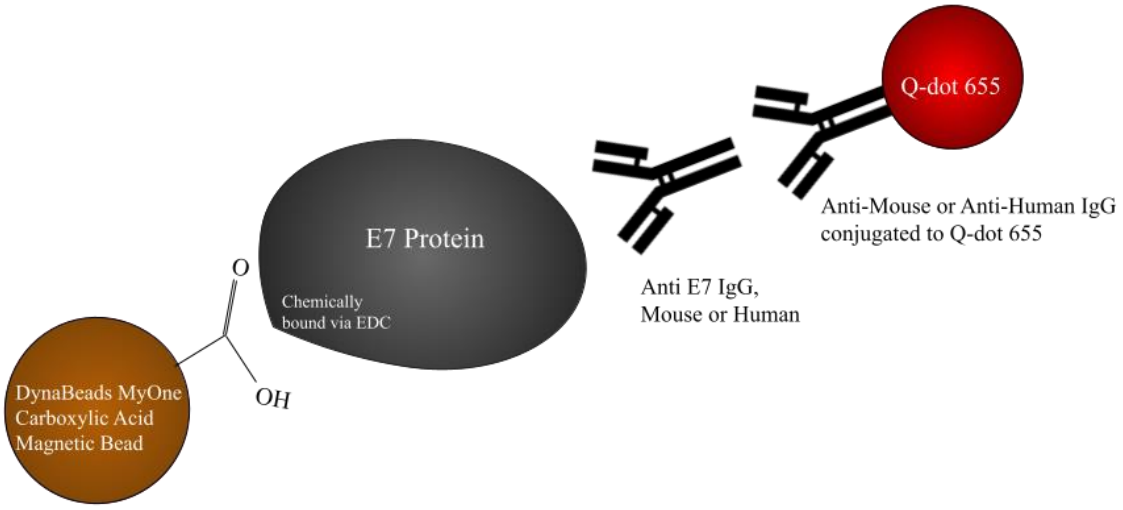

Figure 3: A diagram of the indirect ELISA capture complex.

Sandwich ELISA Proof of Concept

In order to adapt the sandwich ELISA assay to microfluidics, MyOne Carboxylic Acid Dynabeads were conjugated to goat polyclonal anti-GST IgG antibodies in accordance with the protocol found in the product manual from Invitrogen Life Technologies. For proof of concept experiments anti-E7 mouse monoclonal was used to replicate the primary antibody and anti-mouse Fab2' antibody conjugated to Q-dot 655 was used as the secondary antibody. The E7 protein was used at a 1:25 concentration of recombinant E7: 0.1% PBST 0.1% BSA buffer. Taking into account the concentration of the recombinant E7 at ~330 ug/mL, this comes out to approximately 1 ug of recombinant protein added to each reaction. The primary was used at a 1:100 concentration where 1 uL of monoclonal was added to 99 uL of 1x phosphate buffered saline with 0.1% tween and 0.1% BSA, and the secondary was used at a concentration of 1:500 where 1 uL of the antibody was added to 499 uL of 1x phosphate buffered saline with 0.1% tween and 0.1% BSA. The recombinant E7 protein and the primary antibody were applied to the assay in the same step, and the secondary was applied in a second step.

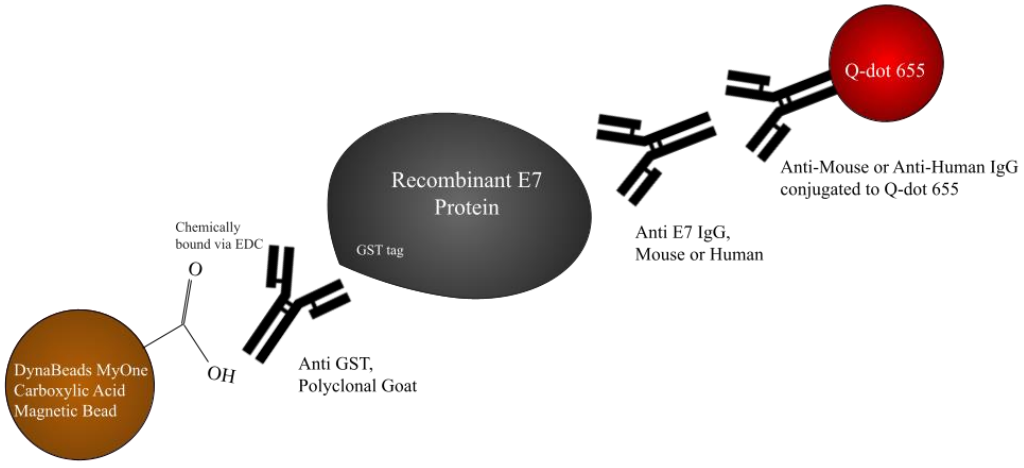

Figure 4: A diagram of the sandwich ELISA capture complex.

On Chip Indirect ELISA

A protocol was established using the microfluidic chips for the indirect ELISA assay. Ten microliters of E7 conjugated MyOne Carboxylic Acid Dynabeads were placed in the 7 layer microfluidic chip with a 3 mm aperture and then were mixed with 15 uL of 1:100 E7 mouse monoclonal antibody suspended in 0.1% PBST 0.1% BSA. The chip was let to sit for 15 minutes. An absorbent pad was used to remove the fluid from the chip via capillary action. A wash step was performed with 20 uL of 0.1% PBST 0.1% BSA. An absorbent pad was used to remove the fluid from the chip and 20 uL of 1:100 Alexa Fluor 488 anti-mouse secondary antibody in 0.1% PBST 0.1% BSA. The chip was covered in foil and let to sit for 15 minutes. A wash step was performed with 20 uL of 0.1% PBST 0.1% BSA. An absorbent pad was used to remove the fluid from the chip via capillary action. An additional 20 ul of 0.1% PBST 0.1% BSA was added to the chip for resuspension before the chip was read in the point of care reader.

Assay Adapting NAPPA to Microfluidics

In Vitro Transcription and Translation

In vitro transcription and translation is a method of expressing protein that utilizes HeLa lysate, accessory proteins, reaction mix, and plasmid DNA incubated at 30 degrees Celsius for a minimum of 90 minutes to create proteins of interest. The plasmid DNA used is the pANT7_cGST plasmid, as described in Ramachandran et al., 2004. The plasmid is a PANT7 vector with a c-terminal GST tag as well as ampicillin and kanamycin resistance. The gene of interest is inserted into the vector through BP and LR reactions. The IVTT reaction uses 0.57 uL of Hela lysate, 0.11 uL of accessory proteins,

0.23 uL of reaction mix, and 0.24 uL of plasmid DNA at a concentration of 200 ng/uL for every 1 uL of protein of interest.

NAPPA Microfluidic Assay Proof of Concept

In order to adapt the sandwich NAPPA assay to microfluidics, MyOne Carboxylic Acid Dynabeads were conjugated to goat polyclonal anti-GST IgG antibodies in accordance with the protocol found in the product manual from Invitrogen Life Technologies. For proof of concept experiments anti-E7 mouse monoclonal was used to replicate the primary antibody and anti-mouse Fab2' antibody conjugated to Q-dot 655 was used as the secondary antibody. The IVTT protein was used at 1:25 concentration of IVTT: 0.1% PBST 0.1% BSA buffer. As the exact concentration of protein made during IVTT cannot be known it is possible there is slight variance in amount of IVTT protein per reaction. The primary was applied with the IVTT E7 and was used at a 1:100 concentration where 1 uL of monoclonal was added to 99 uL of 1x phosphate buffered saline with 0.1% tween 0.1% BSA, and the secondary was used at a concentration of 1:500 where 1 uL of the antibody was added to 499 uL of 1x phosphate buffered saline with 0.1% tween 0.1% BSA.

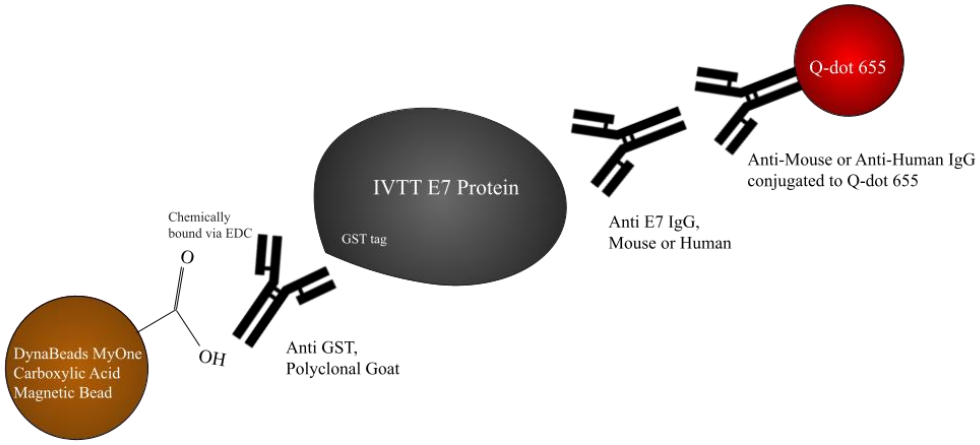

Figure 5: A diagram of the NAPPA sandwich ELISA capture complex.

Magnetics

The magnetic beads used in the assay are the MyOne Carboxylic Acid Dynabeads. The beads are 1 um in size, are non-porous, superparamagnetic, and monodispersed in solution. The beads are made of highly cross-linked polystyrene microspheres and an even dispersion of magnetic material, which is a mixture of maghemite (gamma-Fe2O3) and magnetite (Fe3O4) (Thermo Fisher Scientific, 2015b). The binding capacity of the MyOne Carboxylic Acid Dynabeads is 0.5 ng/uL. Each well in the microfluidic chip contains 10 uL of magnetic beads, amounting to 5 ng of protein or antibody per test condition. In order to utilize a magnetic bead based platform, the microfluidic chips had to be adapted to contain magnetic elements that would enable magnetic beads to remain in place for the assay and be read in the point of care reader.

Magnetic Apertures

Magnetic apertures were created using 8 x 10 adhesive magnetic sheets. A 1 inch by 1 inch square is cut from the sheet and is hole punched to have four 3 mm size magnetic apertures aligned with the four wells of the microfluidic chip. The square is then adhered to the back of the microfluidic chip, aligned to the microfluidic chip wells on the side opposite the in and out flow valves.

Lyophilization

In order to have the magnetic beads remain in place during transport of the assay and in order to increase stability of the magnetic beads over long periods of time the beads were lyophilized. A mixture was created using 10 uL of conjugated magnetic beads with 5 uL of 50% trehalose and 12.5 uL of 20% mannitol for a total pellet volume of 27.5 uL and left to lyophilize overnight.

Study Controls

The plasma controls used in this study are from a pooled sample generated from the HOTSPOT (Human Oral Papillomavirus Transmission in Partners over Time) study, which is reported in Anderson et al, 2015. HPV positive participants, as well as their spouses or partners, and healthy volunteers were enrolled in the HOTSPOT study (Anderson et al., 2015). The samples used in this study were known to be positive for the E7 HPV antigen.

CHAPTER 3

RESULTS

Point of Care Fluorescent Reader for Fluorescence Detection

Fluorophore Comparisons

Multiple fluorophores were tested in order to determine which fluorophore should be used in the assay. Serial dilutions of fluorophores in the red, orange, and green spectra ranges were tested due to compatibility with the point of care reader.

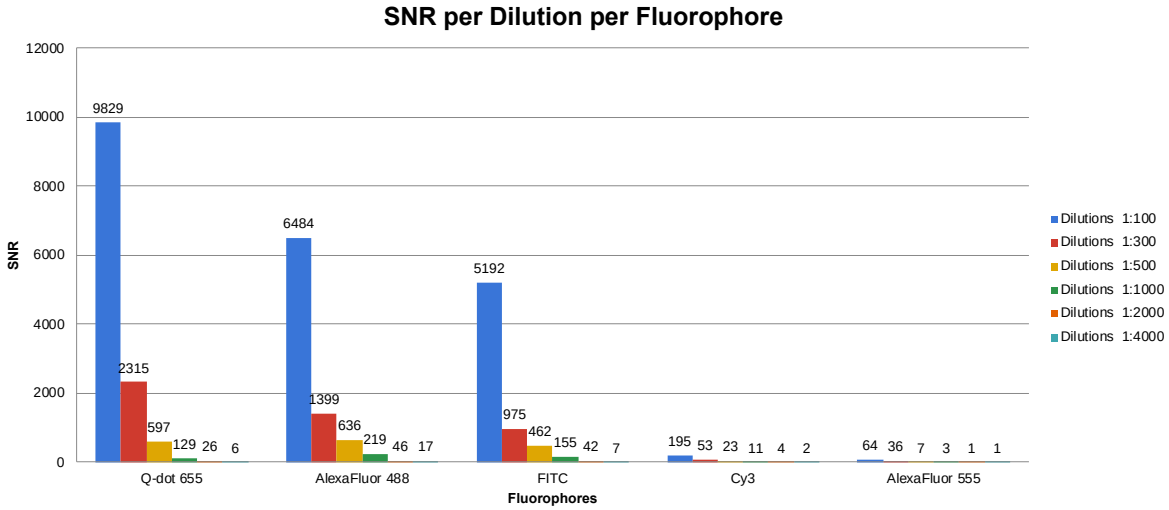

Figure 6: Serial dilutions of Q-dot 655, Alexa Fluor 488, FITC, Cy3, and Alexa Fluor 555 were created at concentrations of 1:100, 1:300, 1:500, 1:1,000, 1:2,000, and 1:4,000 in phosphate buffered saline (PBS). The results were read in the plate reader and a SNR value was generated by measuring the fluorescence of the fluorophore dilution over the fluorescence of the PBS.

Q-dot 655, Alexa Fluor 488, and FITC were chosen for further testing due to the high SNR values found during the serial dilution titration tests. An immunoprecipitation with recombinant E7 conjugated MyOne Carboxylic Acid Dynabeads (the beads/magnetic beads) was performed in order to see the signal generated by the fluorophores in the assay.

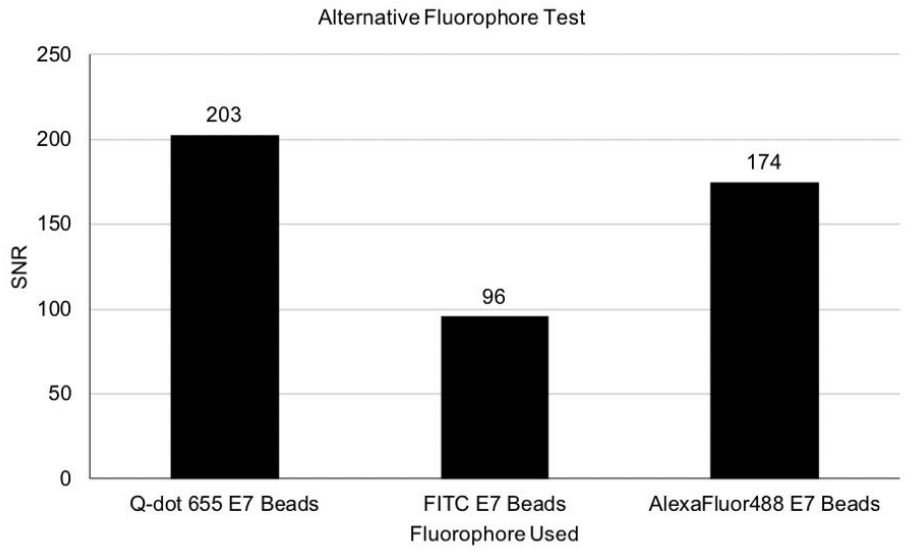

Figure 7: E7 conjugated MyOne Carboxylic Acid Dynabeads were mixed with 200 ng/mL anti-E7 mouse monoclonal for 20 minutes. After one washing step the beads were mixed with either anti-mouse Q-dot 655, Alexa Fluor 488, or FITC at a 1:100 dilution in PBS for an additional 20 minutes. After one washing step the beads were read in the plate reader and SNR was calculated using the fluorescence of the beads over the fluorescence of un-assayed E7 conjugated MyOne Carboxylic Acid Dynabeads.

Q-dot 655 and Alexa Fluor 488 were chosen as the main fluorophores to be used in the assay development. The serial dilutions of the anti-mouse IgG and anti-human IgG conjugations of each fluorophore were read in both the plate reader and the point of care reader.

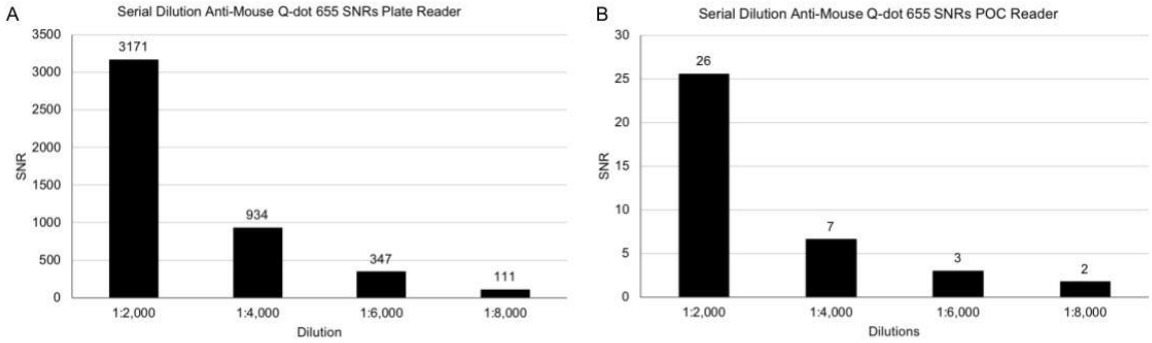

Figure 8: A serial dilution of anti-mouse Q-dot 655 was created at concentrations of 1:2,000, 1:4,000, 1:6,000 and 1:8,000 in phosphate buffered saline (PBS). The results were read in the plate reader (A) and the POC reader (B) and a SNR value was calculated by measuring the fluorescence of the fluorophore dilution over the fluorescence of the PBS.

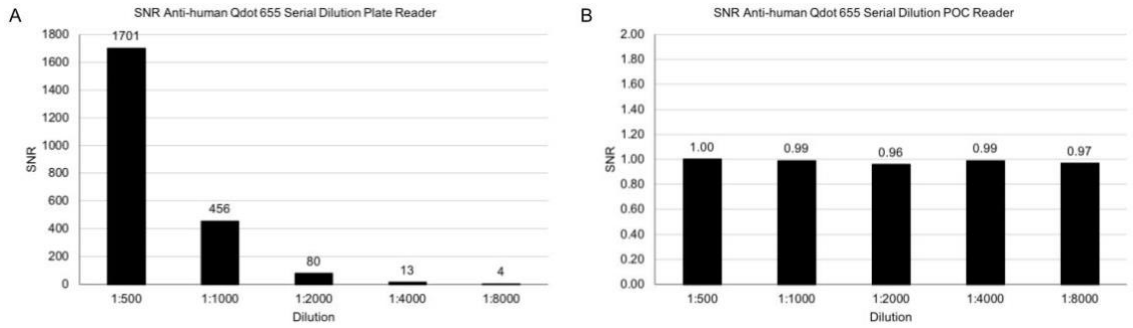

Figure 9: A serial dilution of anti-human Q-dot 655 was created at concentrations of 1:500, 1:1,000, 1:2,000, 1:4,000 and 1:8,000 in phosphate buffered saline (PBS). The results were read in the plate reader (A) and the POC reader (B) and a SNR value was calculated d by measuring the fluorescence of the fluorophore dilution over the fluorescence of the PBS.

The anti-human Q-dot 655 was considerably less bright than the anti-mouse Q-dot 655 and was undetectable in the point of care reader. A replacement vial was requested from Thermo Fisher Scientific and the replacement anti-human Q-dot 655 serial dilution was tested as well.

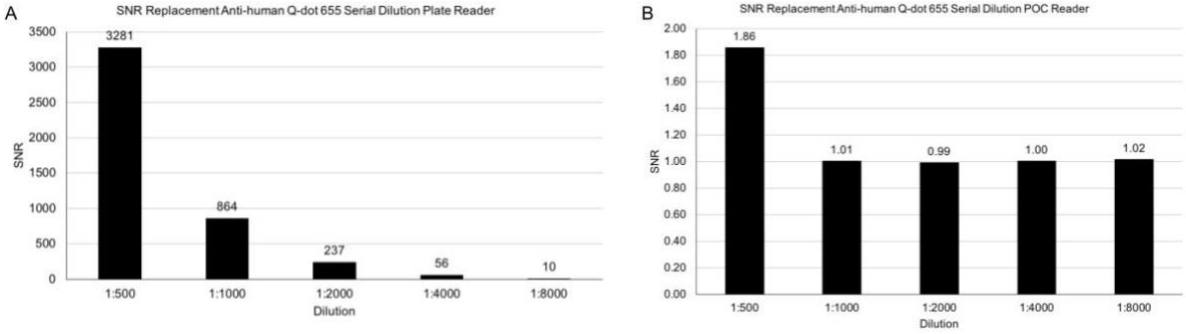

Figure 10: A serial dilution of a replacement vial of anti-human Q-dot 655 was created at concentrations of 1:500, 1:1,000, 1:2,000, 1:4,000 and 1:8,000 in phosphate buffered saline (PBS). The results were read in the plate reader (A) and the POC reader (B) and a SNR value was calculated by measuring the fluorescence of the fluorophore dilution over the fluorescence of the PBS.

The Q-dot 655 replacement vial was considerably brighter than the original vial when read in the plate reader, but the fluorescence was only marginally better when read in the point of care reader. The Q-dot 655 showed large inter-batch variability between conjugated antibodies, which could be problematic for consistency between assays performed.

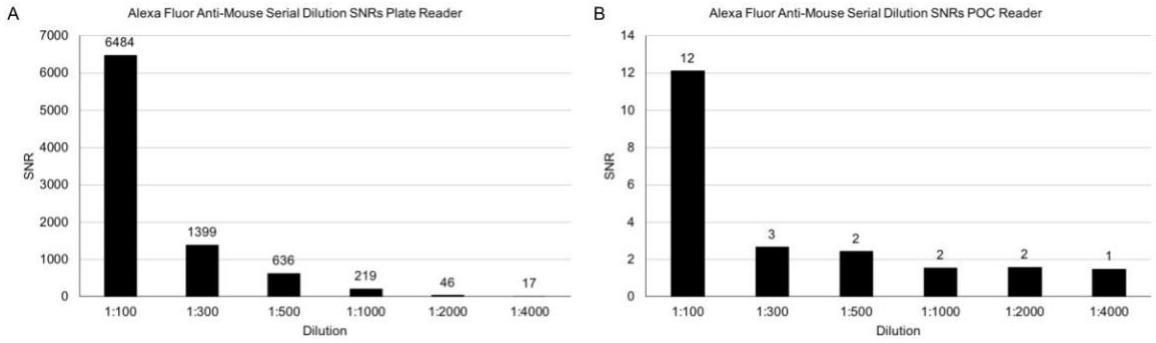

Figure 11: A serial dilution of anti-mouse Alexa Fluor 488 was created at concentrations of 1:100, 1:300, 1:500, 1:1,000, 1:2,000, and 1:4,000 in phosphate buffered saline (PBS). The results were read in the plate reader (A) and the POC reader (B) and a SNR value was calculated by measuring the fluorescence of the fluorophore dilution over the fluorescence of the PBS.

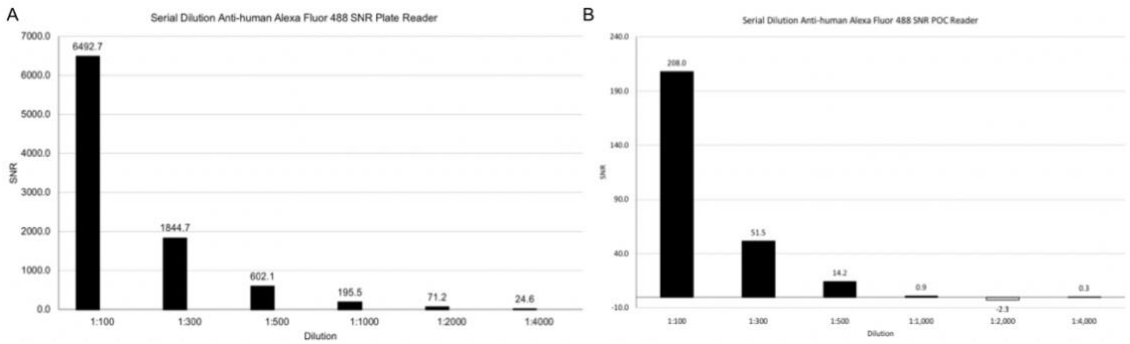

Figure 12: A serial dilution of anti-human Alexa Fluor 488 was created at concentrations of 1:100, 1:300, 1:500, 1:1,000, 1:2,000, and 1:4,000 in phosphate buffered saline (PBS). The results were read in the plate reader (A) and the POC reader (B) and a SNR value was calculated by measuring the fluorescence of the fluorophore dilution over the fluorescence of the PBS.

While the Q-dot 655 anti-mouse outperformed the Q-dot 655 anti-human in terms of fluorescence in both the plate reader and the point of care reader, the Alexa Fluor 488 anti-human outperformed the Alexa Fluor 488 anti-mouse for fluorescence in the plate reader and point of care reader. When working with mouse monoclonal, as in the proof of concept tests, Q-dot 655 could be better to use, and when working with human plasma, Alexa Fluor 488 could be better to use.

The assay is adapted for use with magnetic beads but in order to account for possible future adaptations of the assay, the fluorophores were tested under elution conditions. Pierce Gentle AG/AB Elution Buffer is a near neutral high salt buffer and was

chosen as the elution buffer due to its usefulness in the elution of antibodies without denaturation and inactivation. Elution conditions were tested with the fluorophore in suspension.

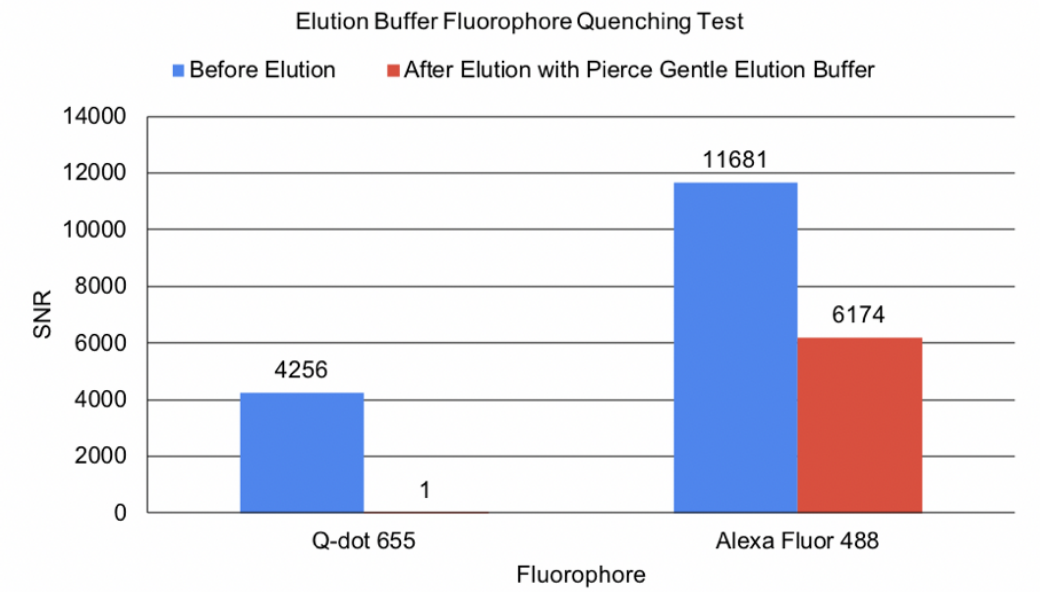

Figure 13: The Q-dot 655 and the Alexa Fluor 488 were measured in the plate reader before the addition of elution buffer and after the addition of elution buffer at a 1:1 ratio. The fluorophores were prepared at a 1:100 dilution in PBS. A SNR was calculated for the before elution values by measuring the fluorescence of the fluorophores over the fluorescence of the PBS. A SNR was calculated for the after elution values by measuring the fluorescence of the fluorophores over the fluorescence of a PBS: Elution buffer mixture at a 1:1 ratio.

Alexa Fluor 488 showed minor quenching upon treatment with the elution buffer and Q-dot 655 showed complete quenching. Alexa Fluor 488 would be best to use for any incorporations of elution steps into the assay.

POC Reader Performance Relative to the Plate Reader

The performance of the point of care reader was compared with the performance of the plate reader. The point of care reader has higher levels of background, which leads to a lower signal output than the plate reader.

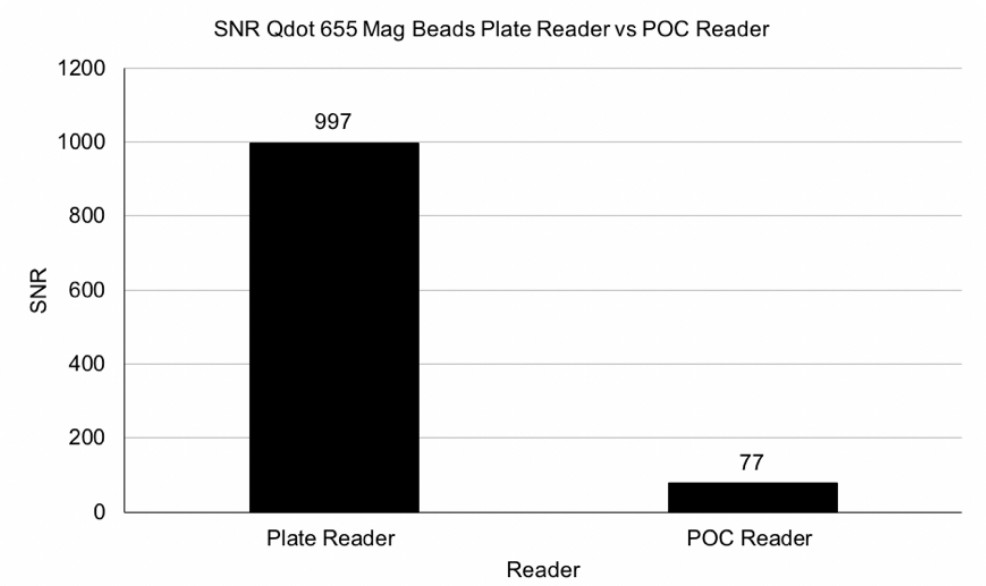

Figure 14: An immunoprecipitation assay with 10 uL of E7 conjugated beads was performed. The beads were mixed with 200 ng/mL anti-E7 mouse monoclonal for 20 minutes. After one washing step the beads were mixed with a dilution of 1:500 anti-mouse Q-dot 655 for an additional 20 minutes. After one washing step the beads were read in the plate reader and point of care reader and SNR was calculated using the fluorescence of the beads over the fluorescence of un-assayed E7 conjugated MyOne Carboxylic Acid Dynabeads.

The autofluorescence of the beads themselves was tested by reading un-assayed E7 conjugated MyOne Carboxylic Acid Dynabeads in suspension in the plate reader and point of care reader and comparing them with assayed beads. The beads exhibited low autofluorescence in suspension and are thought to contribute minimally to any signal generated in the assay.

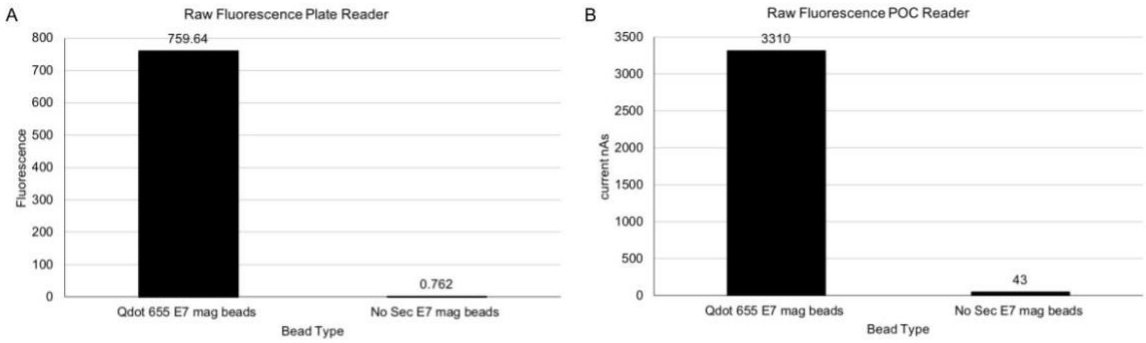

Figure 15: The Q-dot 655 E7 Mag Beads are beads that have been tested in an immunoprecipitation assay, as described in the methods. The No Sec E7 Mag Beads are E7 conjugated MyOne Carboxylic Acid Dynabeads that have not been through an immunoprecipitation assay. The un-assayed beads represent the

autofluorescence of the beads themselves because there is no fluorophore present. The beads were read in the plate reader (A) and the POC reader (B).

Each assay type was performed with plasma samples, the results were read in the plate reader and point of care reader. The point of care reader and the assay will need to be further optimized to reduce background interference before conducting further assays involving plasma samples. Plasma samples naturally have higher background than monoclonal antibodies due to the additional elements that are found mixed within plasma along with the IgG of interest. No further tests were done with plasma beyond comparison tests with the monoclonal antibody.

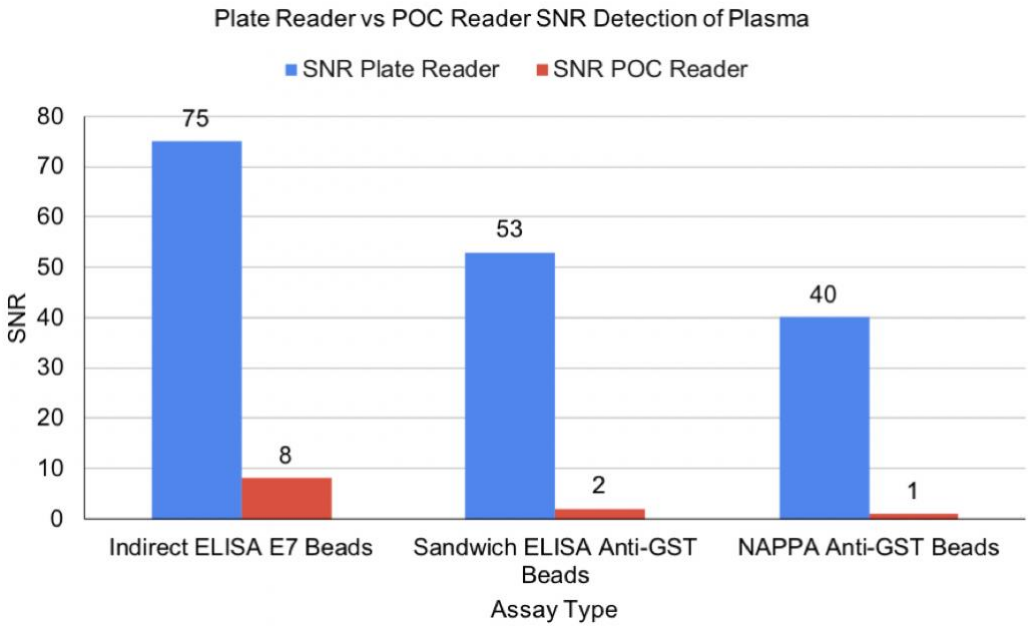

Figure 16: Plasma samples positive for E7 performed with each assay type read in the plate reader vs point of care reader. Each sample was assayed with 10 uL of either E7 conjugated beads or anti-GST conjugated beads, as well as positive plasma. Anti-GST beads were assayed with their respective proteins. Alexa Fluor 488 at a 1:100 concentration was used as the secondary.

Magnetics and Flow Tests

Tests were conducted in order to understand the MyOne Carboxylic Acid Dynabeads (the magnetic beads) intrinsic behavior as well as how they would react under flow conditions and with magnetics.

Bead Behavior

The beads exhibited monodisperse behavior when in suspension. While the beads did settle when left undisturbed, simple agitation such as a shaking movement with the hand would bring them back into a monodisperse state within the suspension.

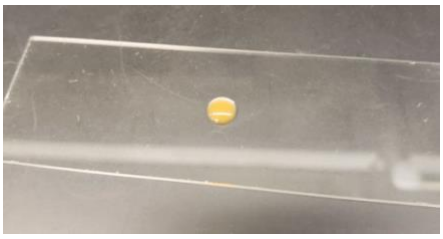

Figure 17: 10 uL of the beads placed as a droplet on a glass slide. The glass slide is approximately 25 mm x 75 mm, the standard size for microscope slides.

The beads were placed in a microfluidic chip and the chip was placed on a magnet. The beads were shown to move with the magnetic force of the magnet whenever the microfluidic chip was moved along the magnet. The beads did not move from their location along the magnet when additional buffer was added to simulate flow conditions.

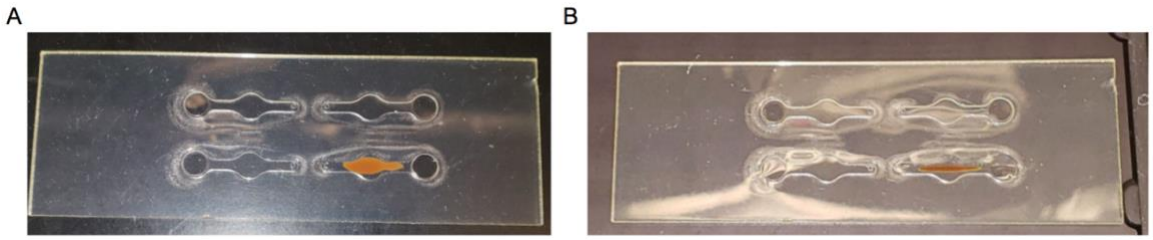

Figure 18: (A) 10 uL of bead suspension was added in the microfluidic chip. At first application the beads were readily dispersing in the suspension within the chip. (B) Once the chip was placed on the magnet the beads formed a close line that moved along with the magnet in whichever direction it was pulled. The magnet was aligned centrally with the microfluidic chip. An additional 10 uL of buffer was added in order to test flow and fill the microfluidic chip. The flow did not alter the bead placement aligned on the magnet. An additional 10 uL was added in order to overflow the chip and the beads did not move under these conditions either. For microfluidic chip dimensions see figure 2.

Tests were conducted in order to see if shaking or agitation was necessary for the binding interactions of the antibodies to the beads. It was found that agitation is not necessary for the binding interaction to take place. This is beneficial for adapting the

assay to the microfluidic chip, as it would be difficult to create agitation of the microfluidic chip in the on chip assay when used in clinical or point of care settings.

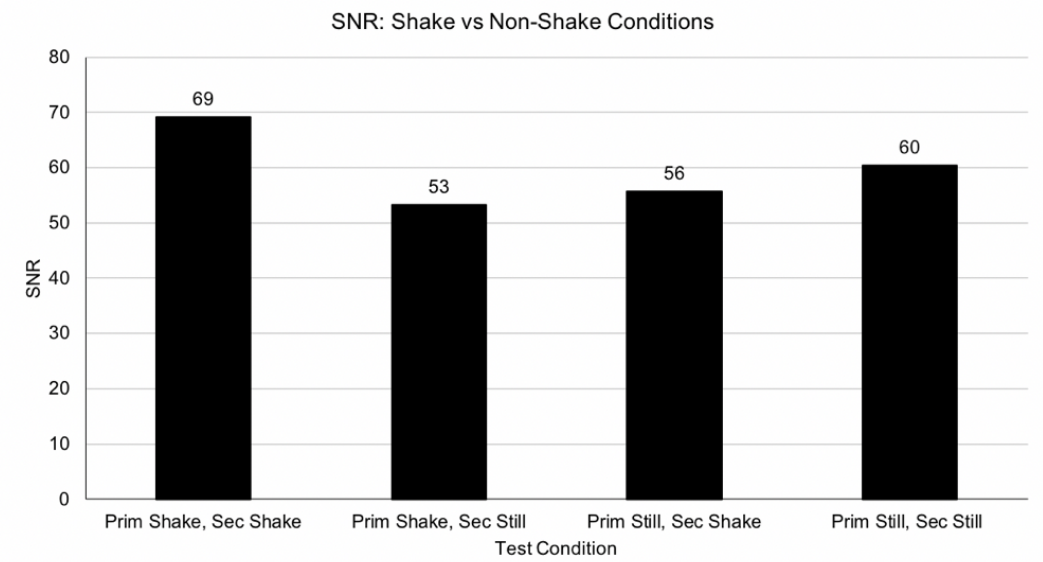

Figure 19: An immunoprecipitation reaction was carried out with 10 uL of E7 conjugated beads. The beads were mixed with 200 ng/mL anti-E7 monoclonal for 20 minutes, were given one wash step, and were then mixed with Q-dot 655 at a 1:500 dilution in 0.1 % PBST 0.1% BSA for 20 minutes and given one final wash before being read in the plate reader. The beads were exposed to four test conditions upon the addition of primary and secondary antibodies. The test conditions were agitation during mixing with the primary antibody and agitation during mixing with the secondary antibody, agitation during mixing with the primary antibody and still during mixing with the secondary antibody, still during mixing with the primary antibody and agitation during mixing with the secondary antibody, and still during mixing with the primary antibody and still during mixing with the secondary antibody.

Microfluidic Magnetics

The microfluidic chip was used for testing the beads under different magnetic conditions. Magnets of two different strengths were tested to see how the beads would interact in simulated flow conditions. The first magnet, 12 mil, had a strength of 200 gauss. The second magnet, 26 mil, had a strength of 350 gauss. The 26 mil magnet was found to be able to hold the beads while the 12 mil magnet was not able to hold the beads.

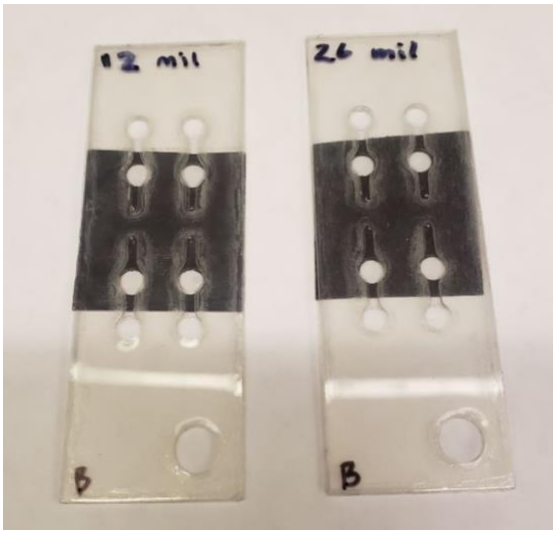

Figure 20: Pictured above is two different magnets adhered to microfluidic 5 layer chips used in magnetic strength tests. The magnet labeled 12 mil is a non-adhesive magnetic strip with 200 gauss and is adhered to the chip with additional plastic adhesive. The magnet labeled 26 mil is an adhesive magnetic strip with 350 gauss and is directly adhered to the chip. The 12 mil magnet is approximately 0.3 mm and the 26 mil magnet is approximately 0.66 mm. For microfluidic chip and magnetic strip dimensions see figure 2. The magnetic strips have a 4mm aperture in the well area.

Under no flow conditions the 12 mil magnet did not appear the exhibit strength against the beads while the 26 mil magnet had some beads localizing to the edges of the magnet, though most remained in the well center. Under flow conditions the 12 mil did not appear to exhibit strength against the beads, and they flowed freely, with most remaining inside the well. The 26 mil magnet under flow conditions was seen to exhibit strength against the beads as more localized to the outer edges of the magnet and less remained in the center of the well. The beads were not seen to flow freely in the 26 mil magnet Under overflow conditions the 12 mil magnet again was not seen to exhibit strength against the beads, and they continued to flow freely, with some remaining in the well center. The 26 mil magnet was seen to exhibit further strength against the beads under overflow conditions and most beads localized to the edges of the magnet Few beads in the 26 mil magnet remained in the well center. The 5 layer chip well capacity appeared to be too thin as some beads in the wells of both microfluidic chips were unable

to flow or move, which may have contributed to the aggregation of some beads within the well center in both the 12 mil and 26 mil microfluidic chips. The 26 mil magnet was chosen as the magnet to be used in the assay.

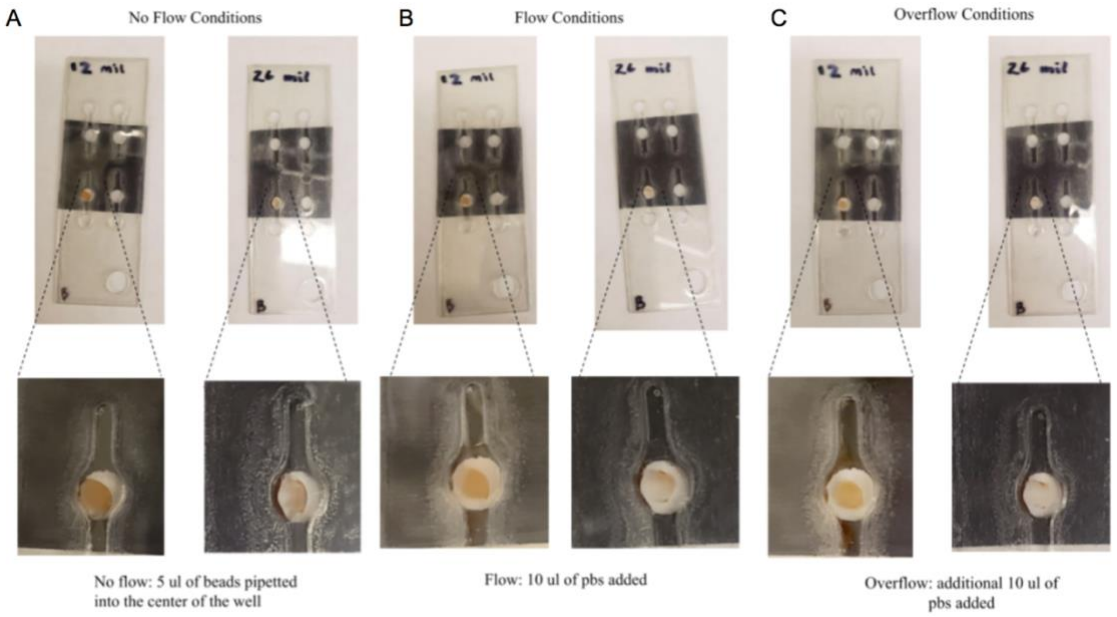

Figure 21: The beads were tested in each magnet type under various simulated flow conditions with a 4mm aperture. (A) No flow conditions represents 5 uL of beads pipetted into the center of the microfluidic chip well. (B) Flow conditions represents the addition of 10 uL of PBS. (C) Overflow conditions represents the addition of a further 10 uL of PBS, which exceeds the volume capacity of the 5 layer chip. For microfluidic chip and magnetic strip dimensions see figure 2.

The 26 mil magnet was used for aperture tests. The apertures were made in the magnet using a hand-held hole punch. Three aperture sizes were tested, the diameters of the apertures were 3 mm, 4 mm, and 5 mm. The diameter size of the microfluidic well is 4 mm. The beads magnetism with each aperture was observed in a 7 layer microfluidic chip.

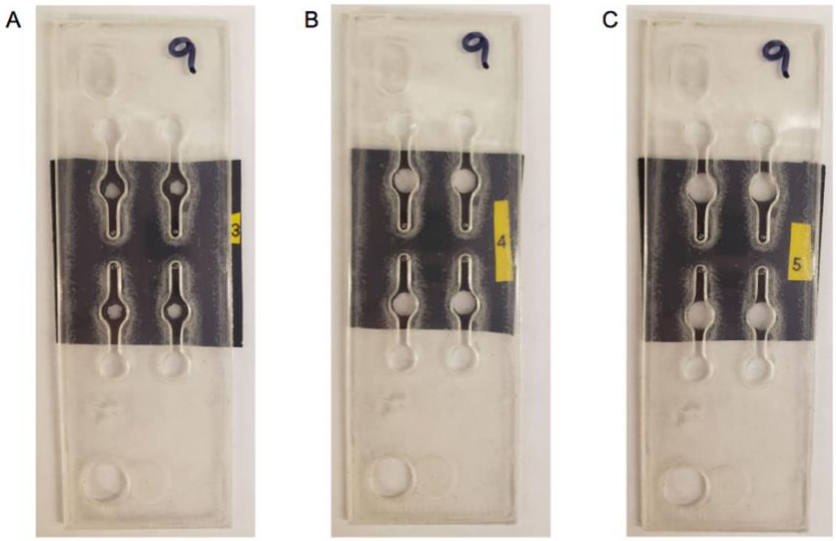

Figure 22: (A) The 3 mm aperture adhered to the microfluidic chip. (B) The 4 mm aperture adhered to the microfluidic chip. (C) The 5 mm aperture adhered to the microfluidic chip. For microfluidic chip and magnetic strip dimensions see figure 2.

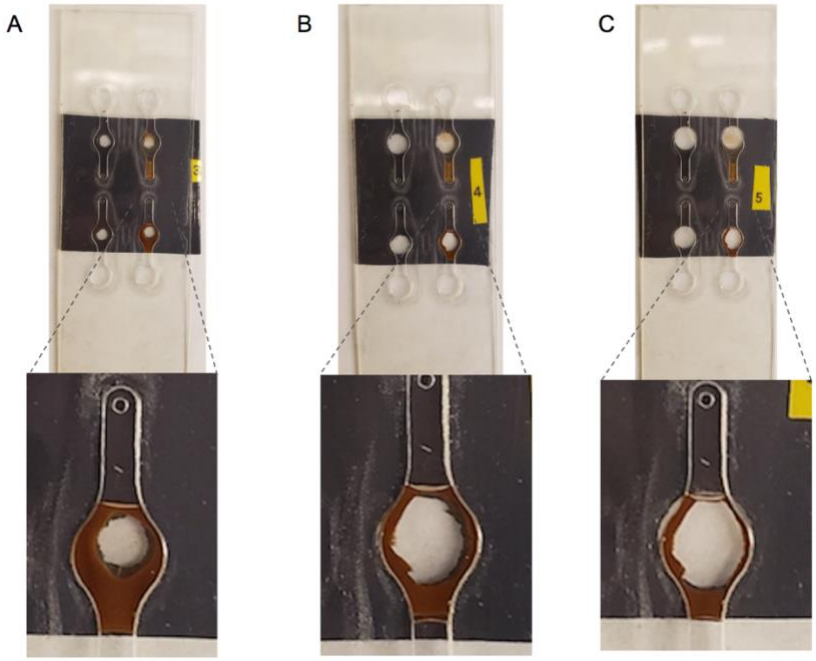

Figure 23: (A) The beads in suspension in the microfluidic chip with the 3 mm aperture adhered. (B) The beads in suspension in the microfluidic chip with the 4 mm aperture adhered. (C) The beads in suspension in the microfluidic chip with the 5 mm aperture adhered. For microfluidic chip and magnetic strip dimensions see figure 2.

Each aperture was tested with E7 conjugated beads that had undergone an immunoprecipitation assay in order to determine which aperture gave the optimum level of signal without interference. The 3 mm aperture gave the highest SNR.

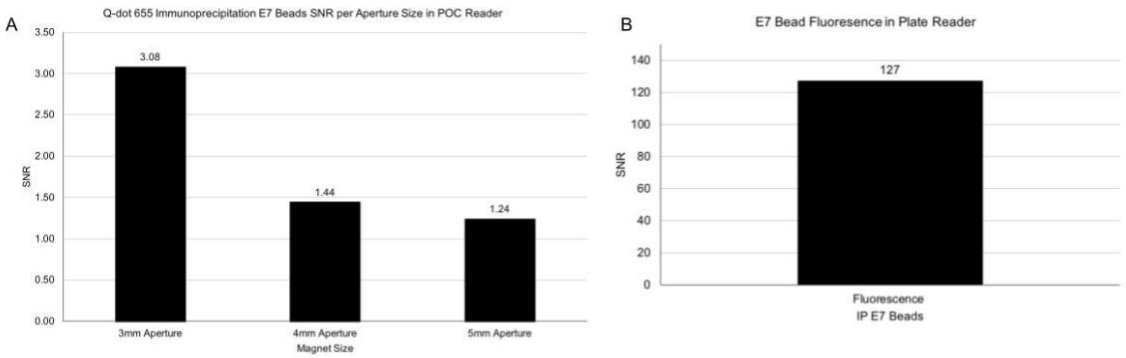

Figure 24: (A) The SNR of 10 uL of E7 conjugated beads that had been assayed in an immunoprecipitation assay as described in the methods tested in each of the apertures and read in the POC reader. (B) The SNR value of the 10 uL of E7 conjugated beads used in the aperture tests read in the plate reader.

The plastic used in the microfluidic chip was found to have some level of autofluorescence. Additionally, the beads opaque nature causes levels of interference with the POC reader detection when they are within the read frame. The microfluidic chip, the microfluidic chip with the 3 mm aperture, and the microfluidic chip with the 3 mm aperture and magnetic beads were tested for autofluorescence. Additionally, air bubbles within the read frame can increase autofluorescence, and the microfluidic chip with the 3 mm aperture, magnetic beads, and a bubble within the read frame was tested.

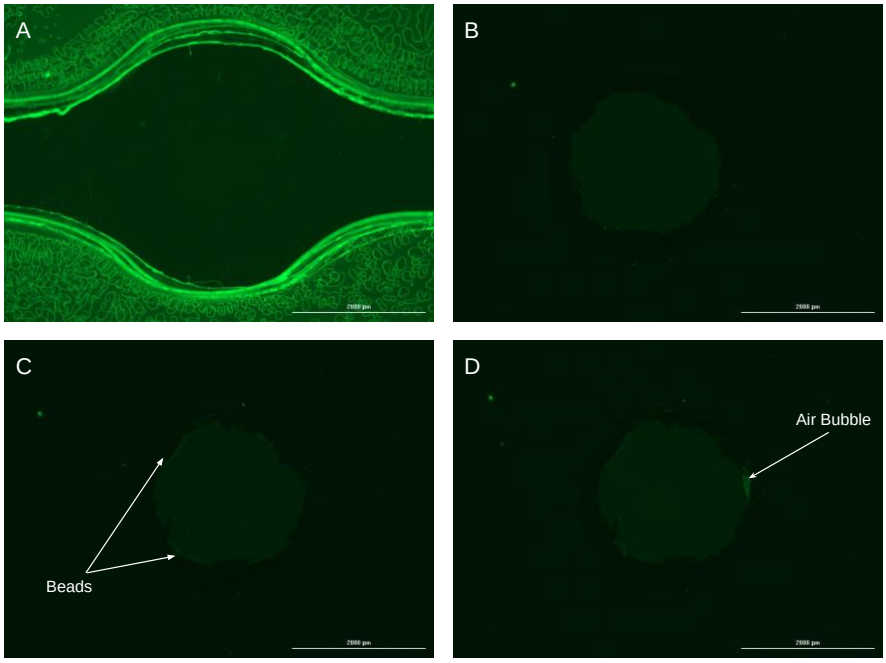

Figure 25: (A) The autofluorescence of the microfluidic chip imaged in Lionheart FX Automated Microscope. (B) The autofluorescence of the microfluidic chip with a 3 mm magnetic aperture imaged in FX Automated Microscope. (C) The autofluorescence of the microfluidic chip with a 3 mm magnetic aperture with 10 uL beads imaged in FX Automated Microscope. (D) The autofluorescence of the microfluidic chip with a 3 mm magnetic aperture with 10 uL beads and an air bubble imaged in FX Automated Microscope. The scale marker line in white indicates 2000 um.

The images of autofluorescence were analyzed in Gen5 version 3.11. The program analyzes a 1000 um diameter circle in the center of the image and calculates fluorescence intensity. The fluorescence intensity was used to determine relative amounts of autofluorescence for each condition.

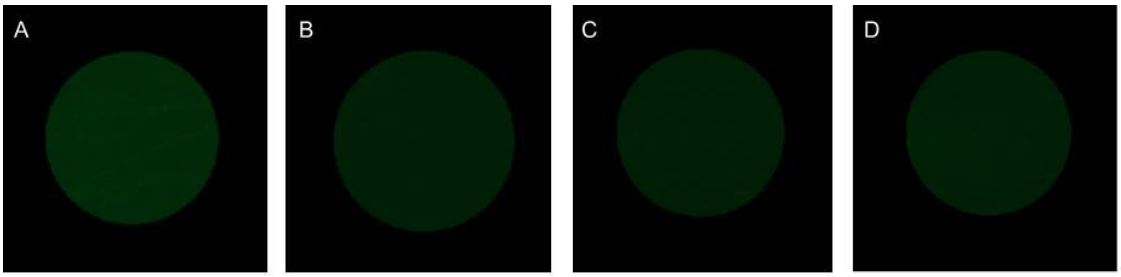

Figure 26: (A) The read area used by Gen5 to measure autofluorescence intensity of the microfluidic chip. (B) The read area used by Gen5 to measure autofluorescence intensity of the microfluidic chip with a 3 mm magnetic aperture. (C) The read area used by Gen5 to measure autofluorescence intensity of the microfluidic chip with a 3 mm magnetic aperture with 10 uL beads. (D) The read area used by Gen5 to measure autofluorescence intensity of the microfluidic chip with a 3 mm magnetic aperture with 10 uL beads and an air bubble.

The autofluorescence of each component of the assay was measured in fluorescence intensity and compared. The average fluorescence intensity of the read area was calculated as well as the standard deviation. The microfluidic chip had high average fluorescence intensity, measuring at 10963 fluorescence units. The 3 mm aperture decreased the average fluorescence intensity by 24.5% to 8278 fluorescence units. It was further decreased by 2.8% to 8049 fluorescence units when the beads were added into the chip with the 3 mm aperture. The air bubble increased the fluorescence units to 8295, an increase of 3.06% over the beads in the chip with the 3mm aperture, and an increase of 0.2% over the chip with the 3mm aperture alone.

Table 1

Autofluorescence Intensity per Assay Component

Value Type	Microfluidic Chip	Microfluidic Chip with 3 mm Aperture	Microfluidic Chip with 3 mm Aperture and Bead Suspension	Microfluidic Chip with 3 mm Aperture and Bubble in Bead Suspension
Mean Fluorescence Intensity	10963	8278	8049	8295
Standard Deviation	688	532	586	596

The autofluorescence affects the ability of the reader to detect signal. Typically, the POC reader SNR is calculated by measuring the sample value over the difference between the sample background and the empty background. The microfluidic chips plastic autofluorescence and the beads interfering behavior when within the POC reader read frame in the 4 mm and 5 mm apertures affected the ability to calculate the SNR value, as the difference between sample background and empty background became a negative value. The relationship between the current of the empty background, sample background, and then known positive samples should always be linear when there is not interfering factors within the read frame. The 3 mm aperture was able to remove the interfering factors of the bead opacity and the plastic autofluorescence from the read frame of the POC reader, leading to a higher signal.

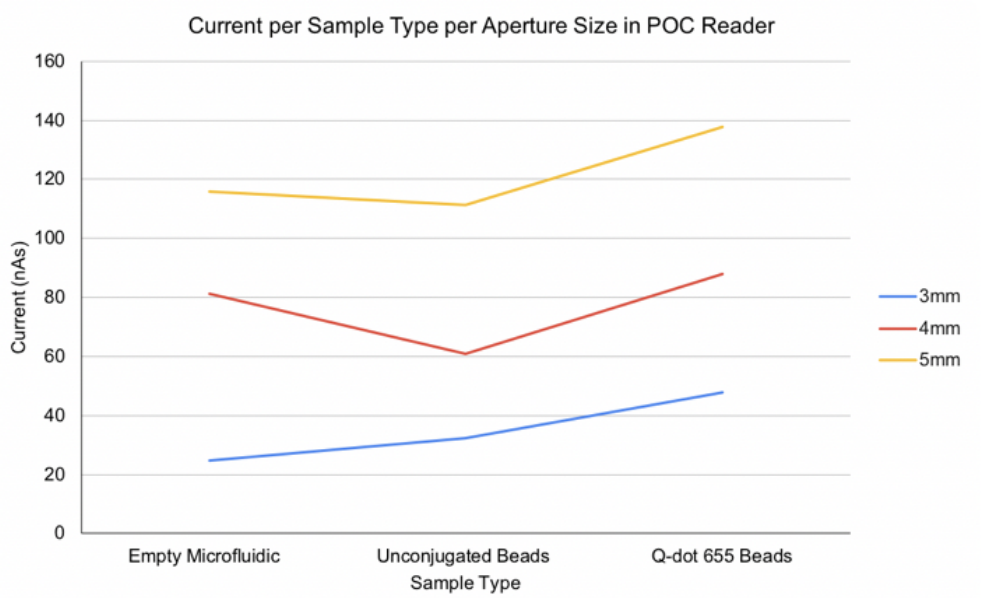

Figure 27: The raw current value in nanoamps of each component used to find the SNR value of the aperture tests.

Assay Adapting ELISA to Microfluidics

Indirect Detection Assay

The Indirect ELISA proof of concept was first tested for optimum buffers. Pierce Gentle AG/AB Binding Buffer and 0.1% PBST 0.1% BSA were both tested in an immunoprecipitation assay. 0.1% PBST 0.1% BSA was chosen as the suspension buffer as it showed higher signal in the tested immunoprecipitation assay.

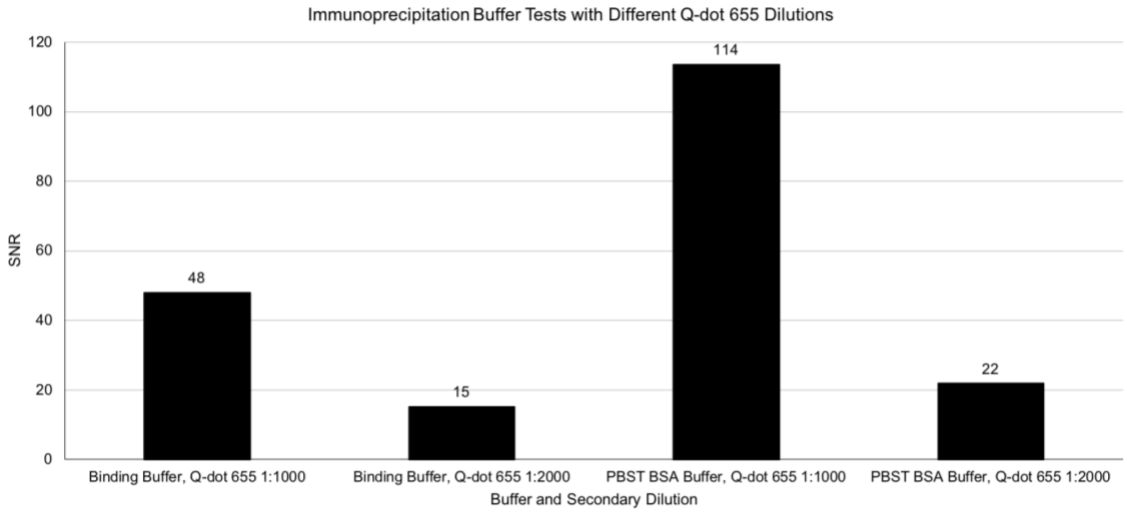

Figure 28: An immunoprecipitation reaction was carried out with test conditions using 10 uL of E7 conjugated beads per test. The beads were mixed with 200 ng/mL anti-E7 monoclonal for 40 minutes, were given one wash step, and were then mixed with Q-dot 655 at a 1:1000 or 1:2000 dilution in PBS for 40 minutes and given one final wash before being read in the plate reader. The beads were exposed to two test conditions, suspension in Pierce Gentle AG/AB Binding Buffer or 0.1% PBST 0.1% BSA.

Next in the development of the assay, a limit of detection test was carried out. The limits of detection assay is an analysis of the lowest concentration of analyte in a sample that is detected consistently (Vashist & Luong, 2018). A limit of detection analysis was performed with varying known concentrations of monoclonal antibody, as well as with varying known concentrations of monoclonal antibody spiked into negative plasma. Spiking monoclonal antibodies into negative plasma samples gives an idea of how much background signal in the assay comes from components in the plasma that are not the antibody of interest.

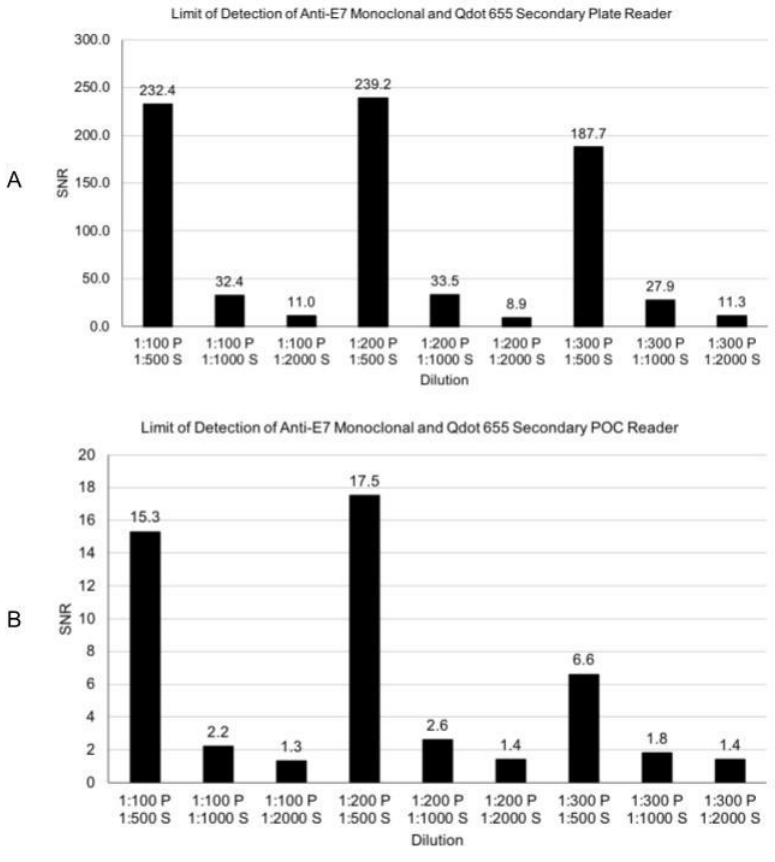

Figure 29: An immunoprecipitation reaction was carried out with test conditions using 10 uL of E7 conjugated beads per test. The beads were mixed with 200 ng/mL (1:100) anti-E7 monoclonal, 100 ng/mL (1:200) anti-E7 monoclonal, or 75 ng/mL (1:300) anti-E7 monoclonal, for 40 minutes, were given one wash step, and were then mixed with Q-dot 655 at a 1:500, 1:1000, or 1:2000 dilution in 0.1% PBST 0.1% BSA for 40 minutes and given one final wash before being read in the plate reader and point of care reader.

A concentration of 1:500 was chosen for the Q-dot 655 secondary as the signal was most detectable using that concentration. The signal at that secondary concentration remained high at the 200 ng/mL (1:100) anti-E7 monoclonal, 100 ng/mL (1:200) anti-E7 monoclonal, and 75 ng/mL (1:300) anti-E7 monoclonal primary concentrations.

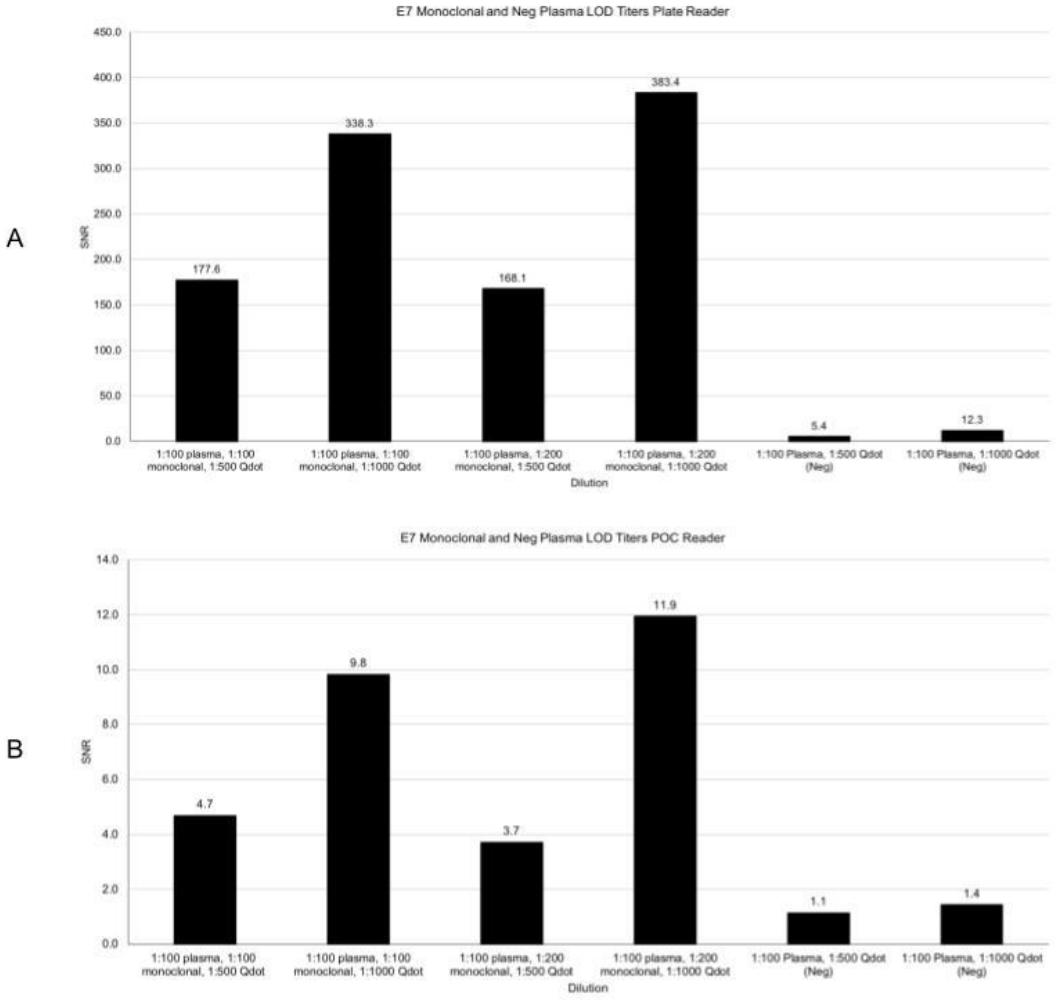

Figure 30: An immunoprecipitation reaction was carried out with test conditions using 10 uL of E7 conjugated beads per test. The beads were mixed with 1 uL of plasma and 200 ng/mL (1:100) anti-E7 monoclonal, 100 ng/mL (1:200) anti-E7 monoclonal, or no anti-E7 monoclonal for 40 minutes, were given one wash step, and were then mixed with Q-dot 655 at a 1:500 or 1:1000 dilution in 0.1% PBST 0.1% BSA for 40 minutes and given one final wash before being read in the plate reader and point of care reader.

It is possible that the hook effect is shown in the 1:100 dilutions of the monoclonal antibody tested beads. The hook effect is a common limitation of immunoassays and it occurs when an excess amount of analytes of interest give falsely low results (Zhang, 2015).

Plasma in immunoassays will almost always give lower signals than monoclonal antibodies. Monoclonal antibodies are specifically raised against antigens in near optimal conditions during industrial production, they also go through quality control procedures, while antibodies in plasma occur from the human immune response. It is important to recognize that the expected signal might decrease when transitioning the proof of concept assay using monoclonal antibodies to a diagnostic assay using human plasma.

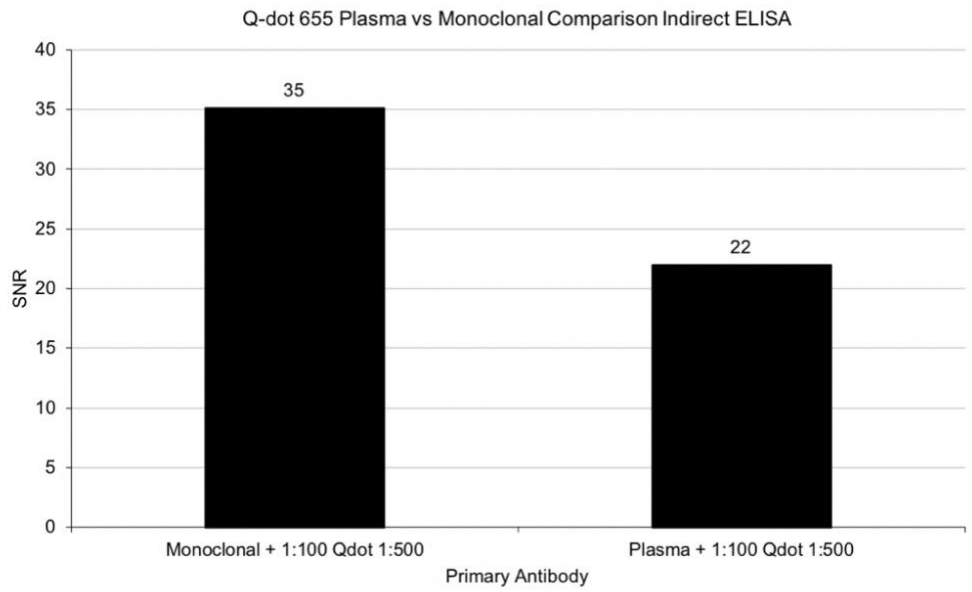

Figure 31: An immunoprecipitation reaction was carried out with test conditions using 10 uL of E7 conjugated beads per test. The beads were mixed with 1 uL of plasma or 200 ng/mL (1:100) anti-E7 monoclonal for 20 minutes, were given one wash step, and were then mixed with Q-dot 655 at a 1:500 dilution in 0.1% PBST 0.1% BSA for 20 minutes and given one final wash before being read in the plate reader.

The monoclonal and plasma comparisons were carried out using both 1:500 Q-dot 655 and Alexa Fluor 488 as the secondary antibodies. The Alexa Fluor 488 anti-human

fluorophore performs better for this test, as was expected based on the results of the fluorophore serial dilutions. The monoclonal SNR is 2.32 times higher than the plasma SNR.

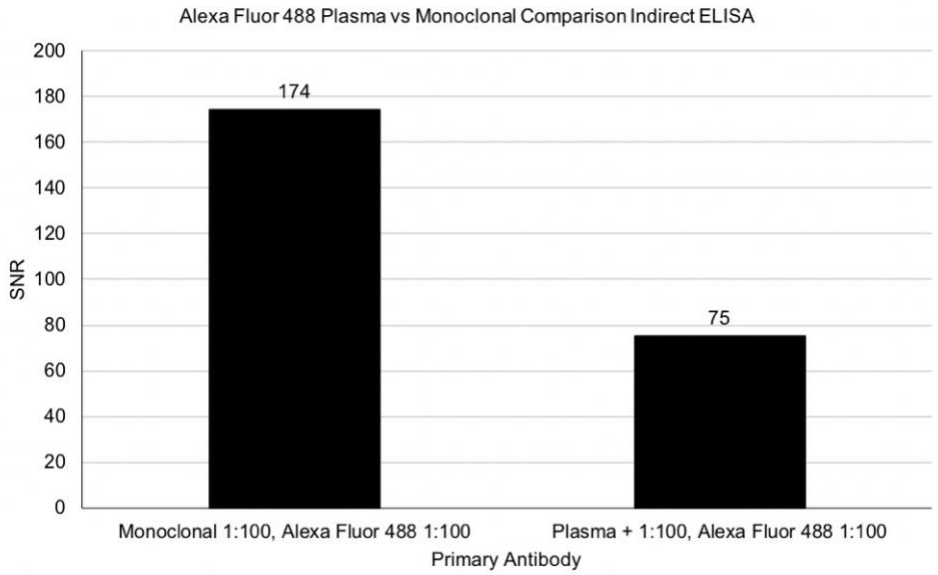

Figure 32: An immunoprecipitation reaction was carried out with test conditions using 10 uL of E7 conjugated beads per test. The beads were mixed with 1 uL of plasma or 200 ng/mL (1:100) anti-E7 monoclonal for 20 minutes, were given one wash step, and were then mixed with Alexa Fluor 488 at a 1:100 dilution in 0.1% PBST 0.1% BSA for 20 minutes and given one final wash before being read in the plate reader.

Sandwich Detection Assay

Before testing the proof of concept assay for the Sandwich ELISA, the anti-GST goat polyclonal antibody conjugated to the beads was validated with a plate ELISA assay.

Table 2

Plate ELISA Anti-GST Capture of Recombinant E7

Sample	SNR (Over Plate Background)	SNR (Over Secondary Background)
Recombinant E7 Full Immunoprecipitation	2960.59	1489.25
Recombinant E7 Secondary Only	1.99	

The plate ELISA validated that the anti-GST capture antibody conjugated to the beads was functioning correctly and capturing the analyte. An immunoprecipitation with the anti-GST conjugated beads was performed using recombinant E7 with a C terminal GST tag. The immunoprecipitation using anti-GST conjugated magnetic beads performed similarly to the immunoprecipitation using E7 conjugated magnetic beads.

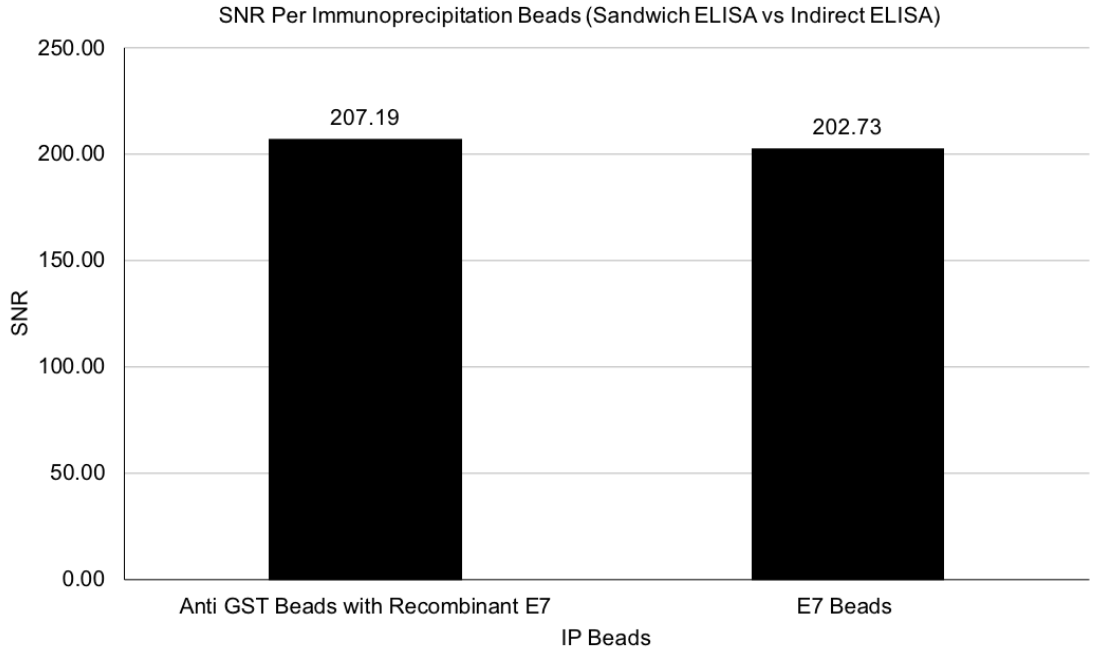

Figure 33: An immunoprecipitation reaction was carried out with test conditions using 10 uL of E7 conjugated beads or anti-GST conjugated beads. The E7 beads were mixed with 200 ng/mL (1:100) anti-E7 monoclonal for 20 minutes, were given one wash step, and were then mixed with Q-dot 655 at a 1:500 dilution in 0.1% PBST 0.1% BSA for 20 minutes and given one final wash before being read in the plate reader. The anti-GST beads were mixed with 200 ng/mL (1:100) anti-E7 monoclonal and 1 ug (4 uL) of recombinant E7 protein for 20 minutes, were given one wash step, and were then mixed with Q-dot 655 at a 1:500 dilution in 0.1% PBST 0.1% BSA for 20 minutes and given one final wash before being read in the plate reader.

A limit of detection assay was carried out using Alexa Fluor 488. Primary monoclonal concentrations of 200 ng/mL (1:100) anti-E7 monoclonal and 100 ng/mL (1:200) anti-E7 monoclonal were tested, as well as secondary concentrations of 1:100 and 1:300 in 0.1% PBST 0.1% BSA. The Alexa Fluor 488 is used in these tests as it was determined during the indirect ELISA testing that Alexa Fluor 488 performs better than

the Q-dot 655 in the immunoprecipitation assay. The assay has strong SNR at all primary and secondary concentrations tested.

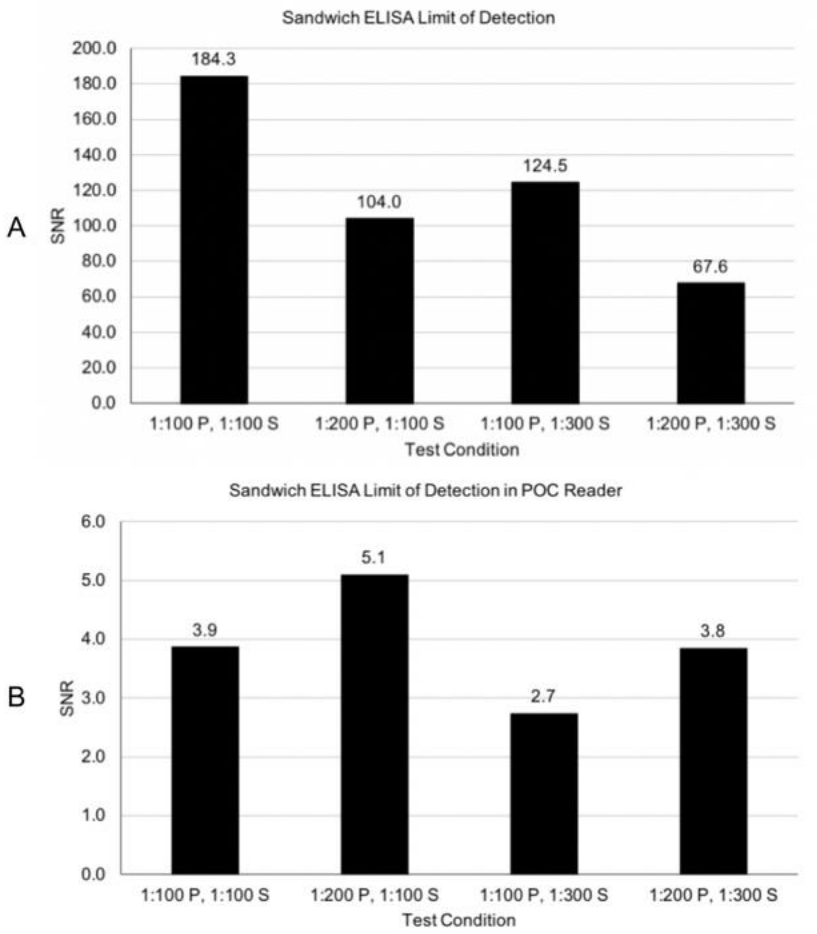

Figure 34: An immunoprecipitation reaction was carried out with test conditions using 10 uL of anti-GST conjugated beads per test. The beads were mixed with 200 ng/mL (1:100) anti-E7 monoclonal or 100 ng/mL (1:200) anti-E7 monoclonal with 1 ug (4uL) recombinant E7 protein for 20 minutes, were given one wash step, and were then mixed with Alexa Fluor 488 at a 1:100 or 1:300 dilution in 0.1% PBST 0.1% BSA for 20 minutes and given one final wash before being read in the plate reader (A) and point of care reader (B).

A comparison between the monoclonal and plasma was carried out for the sandwich ELISA assay. Alexa Fluor 488 was used as the secondary for these immunoprecipitations. The monoclonal SNR was 3.47 times higher than the plasma SNR. The difference in signal generated from the monoclonal and plasma immunoprecipitation tests is higher in the anti-GST conjugated beads using recombinant E7 than in the E7

conjugated beads. It is possible that the anti-GST beads generate higher background noise than the E7 conjugated beads.

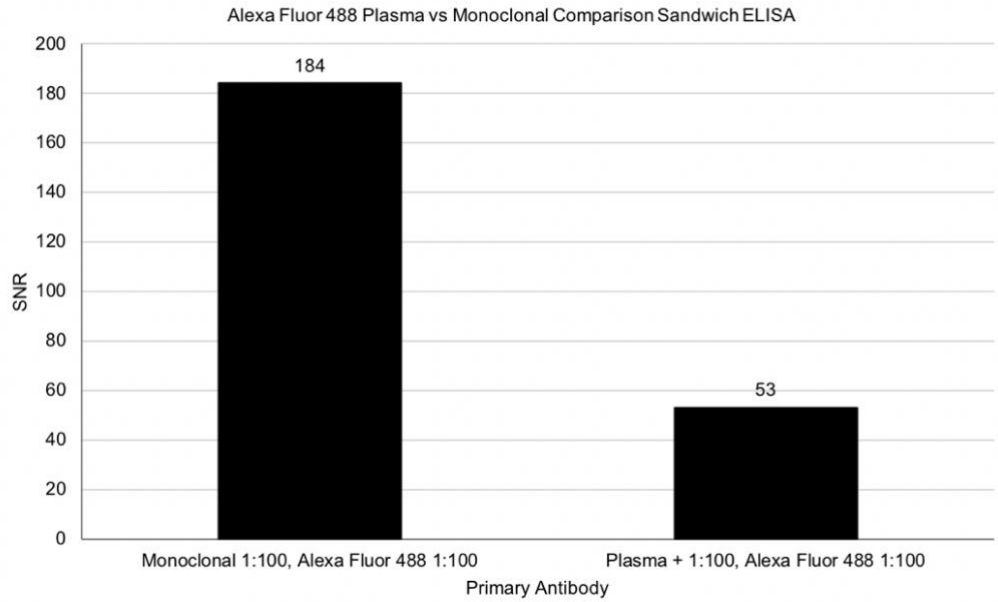

Figure 35: An immunoprecipitation reaction was carried out with test conditions using 10 uL of anti-GST conjugated beads per test. The beads were mixed with 1 uL of plasma or 200 ng/mL (1:100) anti-E7 monoclonal and 1 ug (4 uL) of recombinant E7 protein for 20 minutes, were given one wash step, and were then mixed with Alexa Fluor 488 at a 1:100 dilution in 0.1% PBST 0.1% BSA for 20 minutes and given one final wash before being read in the plate reader.

Assay Adapting NAPPA to Microfluidics

Sandwich Detection Assay

Before testing the proof of concept assay for the NAPPA Sandwich ELISA, the anti-GST goat polyclonal antibody conjugated to the beads was validated with a plate ELISA assay.

Table 3

Plate ELISA Anti-GST Capture of IVTT E7

Sample	SNR (Over Plate Background)	SNR (Over Secondary Background)
IVTT E7 Full Immunoprecipitation	5022.37	854.83
IVTT E7 Secondary Only	5.88	

The plate ELISA validated that the anti-GST capture antibody conjugated to the beads was functioning correctly and capturing the analyte. It is important to note that the IVTT proteins have higher background than the recombinant proteins (as discussed in Table 2). The background can be seen in the test conducted with only capture antibody, protein, and secondary antibody (IVTT E7 Secondary Only). No primary antibody was used in this test, so the signal is the interaction between the secondary and the protein. The IVTT E7 Secondary Only SNR was 295% higher than the Recombinant E7 Secondary Only SNR (Table 2), indicating a much higher background caused by the secondary antibody interactions with the protein analyte. Higher background with IVTT created proteins could be due to the reagents used during protein expression.

An immunoprecipitation with the anti-GST conjugated beads was performed using IVTT expressed E7 with a C terminal GST tag. The anti-GST conjugated beads had a lower immunoprecipitation SNR than the E7 conjugated beads. This could be due to the higher background signal generated when working with IVTT proteins.

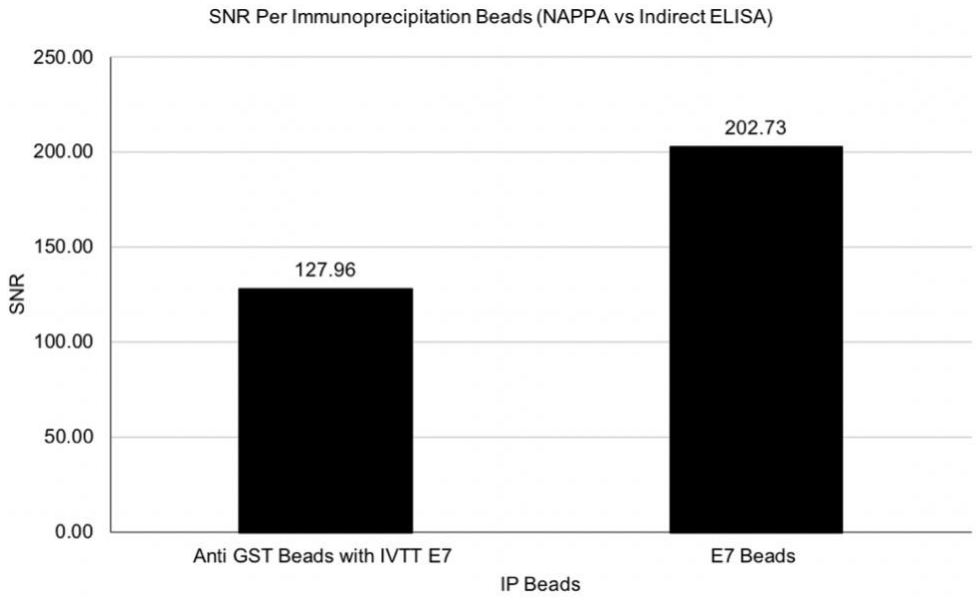

Figure 36: An immunoprecipitation reaction was carried out with test conditions using 10 uL of E7 conjugated beads or anti-GST conjugated beads. The E7 beads were mixed with 200 ng/mL (1:100) anti-E7 monoclonal for 20 minutes, were given one wash step, and were then mixed with Q-dot 655 at a 1:500 dilution in 0.1% PBST 0.1% BSA for 20 minutes and given one final wash before being read in the plate reader. The anti-GST beads were mixed with 200 ng/mL (1:100) anti-E7 monoclonal and IVTT expressed E7 at a 1:25 concentration (4 uL) for 20 minutes, were given one wash step, and were then mixed with Q-dot 655 at a 1:500 dilution in 0.1% PBST 0.1% BSA for 20 minutes and given one final wash before being read in the plate reader.

A limit of detection assay was carried out using Alexa Fluor 488. Primary monoclonal concentrations of 200 ng/mL (1:100) anti-E7 monoclonal and 100 ng/mL (1:200) anti-E7 monoclonal were tested, as well as secondary concentrations of 1:100 and 1:300 in 0.1% PBST 0.1% BSA. The assay has strong SNR at all primary and secondary concentrations tested.

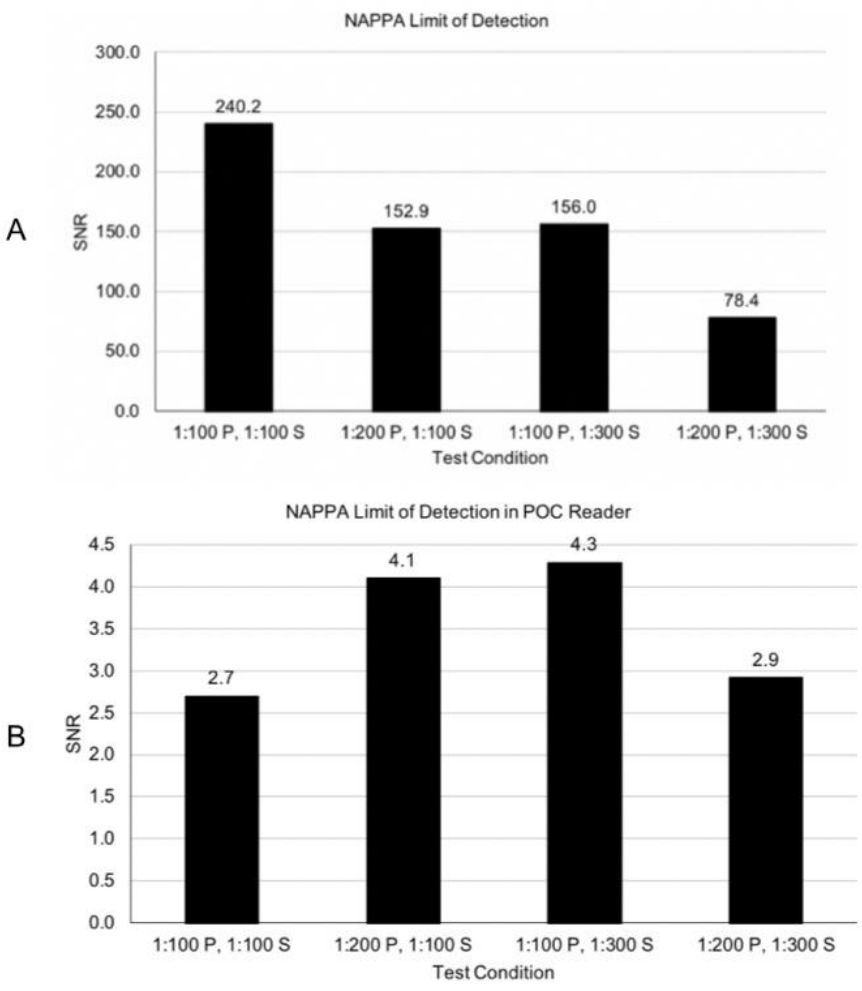

Figure 37: An immunoprecipitation reaction was carried out with test conditions using 10 uL of anti-GST conjugated beads per test. The beads were mixed with 200 ng/mL (1:100) anti-E7 monoclonal or 100 ng/mL (1:200) anti-E7 monoclonal with 1:25 concentration (4uL) IVTT E7 protein for 20 minutes, were given one wash step, and were then mixed with Alexa Fluor 488 at a 1:100 or 1:300 dilution in 0.1% PBST 0.1% BSA for 20 minutes and given one final wash before being read in the plate reader (A) and point of care reader (B).

A comparison between the monoclonal and plasma was carried out for the sandwich ELISA assay. Alexa Fluor 488 was used as the secondary for these immunoprecipitations. The monoclonal SNR was 3.45 times higher than the plasma SNR. The difference in signal generated from the monoclonal and plasma immunoprecipitation tests is again higher in the anti-GST conjugated beads using IVTT E7 than in the E7 conjugated beads. This could again be due to possibility that the anti-GST beads generate higher background noise than the E7 conjugated beads.

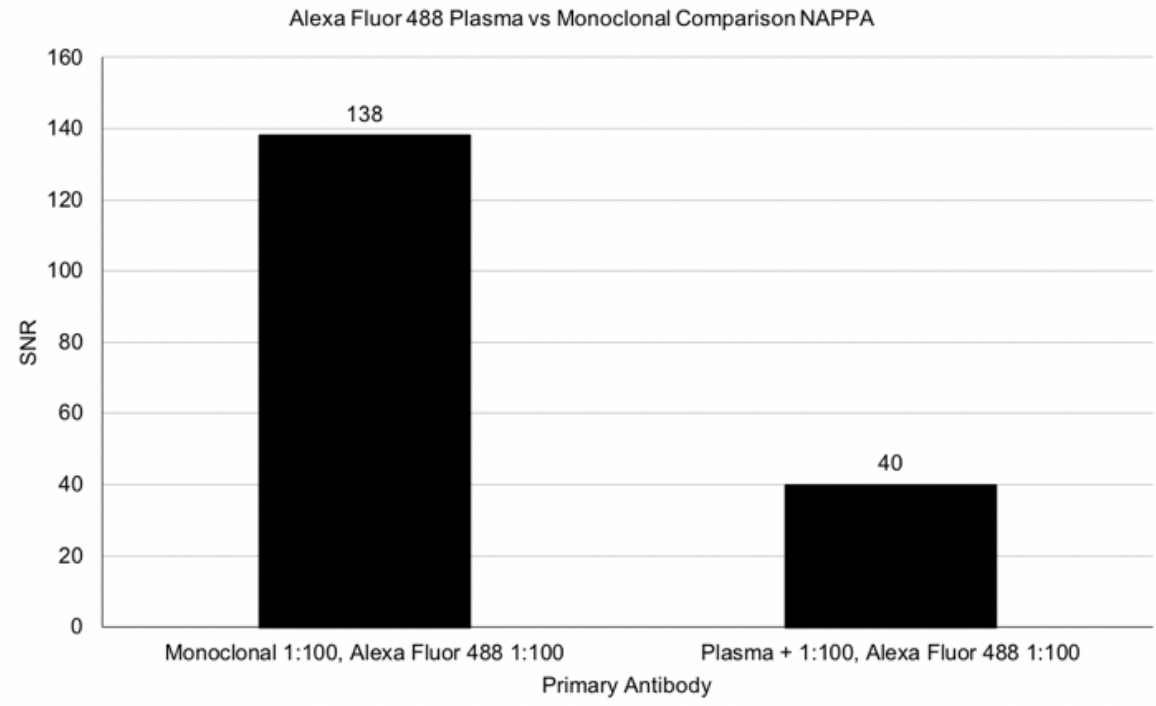

Figure 38: An immunoprecipitation reaction was carried out with test conditions using 10 uL of anti-GST conjugated beads per test. The beads were mixed with 1 uL of plasma or 200 ng/mL (1:100) anti-E7 monoclonal and IVTT E7 protein at a concentration of 1:25 (4 uL) for 20 minutes, were given one wash step, and were then mixed with Alexa Fluor 488 at a 1:100 dilution in in 0.1% PBST 0.1% BSA for 20 minutes and given one final wash before being read in the plate reader.

Drying of Magnetic Beads

Bead Stability

An important aspect of the assay is stability over time. The protein conjugated beads were tested in liquid suspension state and in dried state in order to optimize conjugated bead storage. The protein conjugated beads in the liquid suspension state can be susceptible to degradation, microbial contamination, or protease activity. The beads when stored in liquid suspension were shown to lose signal over time.

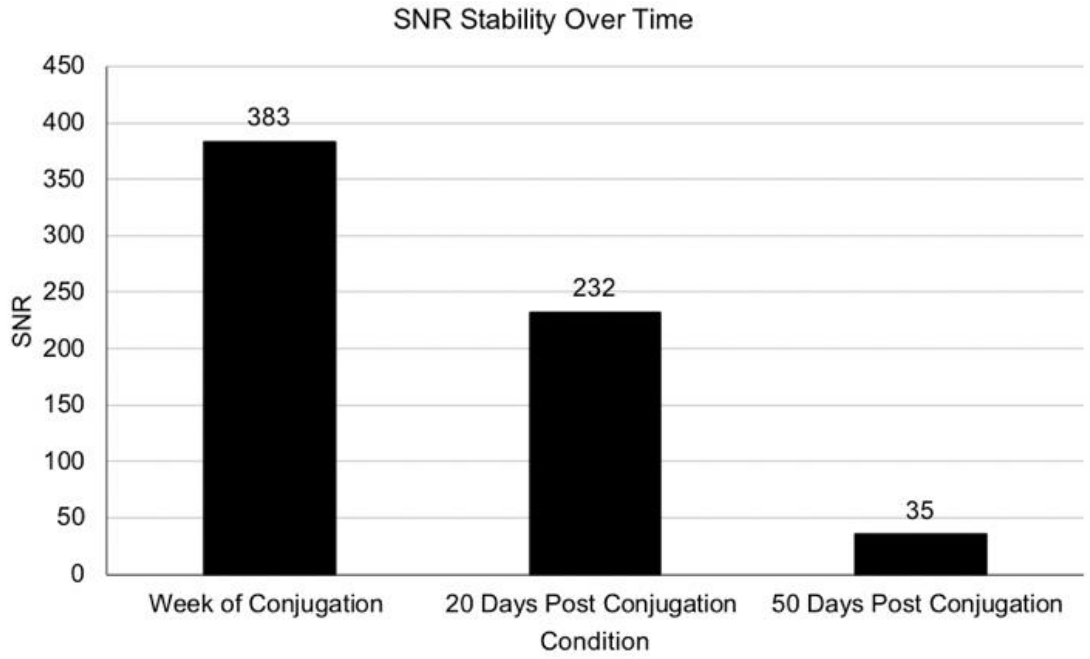

Figure 39: Stability of the conjugated beads over time. Immunoprecipitation assays were performed with 10 uL of E7 conjugated beads, 200 ng/mL of anti E7 mouse monoclonal, and 1:500 anti-mouse Q-dot 655. The immunoprecipitations were performed at various time points to determine loss of signal over time.

The E7 conjugated beads lost signal over time with liquid suspension storage. After 20 days from the conjugation date the signal decreased 39%. After 50 days from the conjugation date the signal decreased 91% from the week of conjugation signal and 85% from the 20 day signal. It was necessary to find a way to keep protein conjugated beads stable in order to decrease signal loss over time. Liquid suspension storage of proteins is

particularly prone to protein degradation over time through oxidation, proteolysis by proteolytic enzymes, or microbial contamination over dried or pelleted storage.

Vacuum Centrifugation

Vacuum centrifugation of E7 conjugated beads was done in order to create stable bead pellets. The E7 conjugated beads were tested in immunoprecipitation assays in order to determine the effect of vacuum centrifugation on the beads and if they remained stable over time. The E7 conjugated beads were dried at 30 degrees Celsius for 1 hour under vacuum centrifugation conditions in order to create the bead pellets.

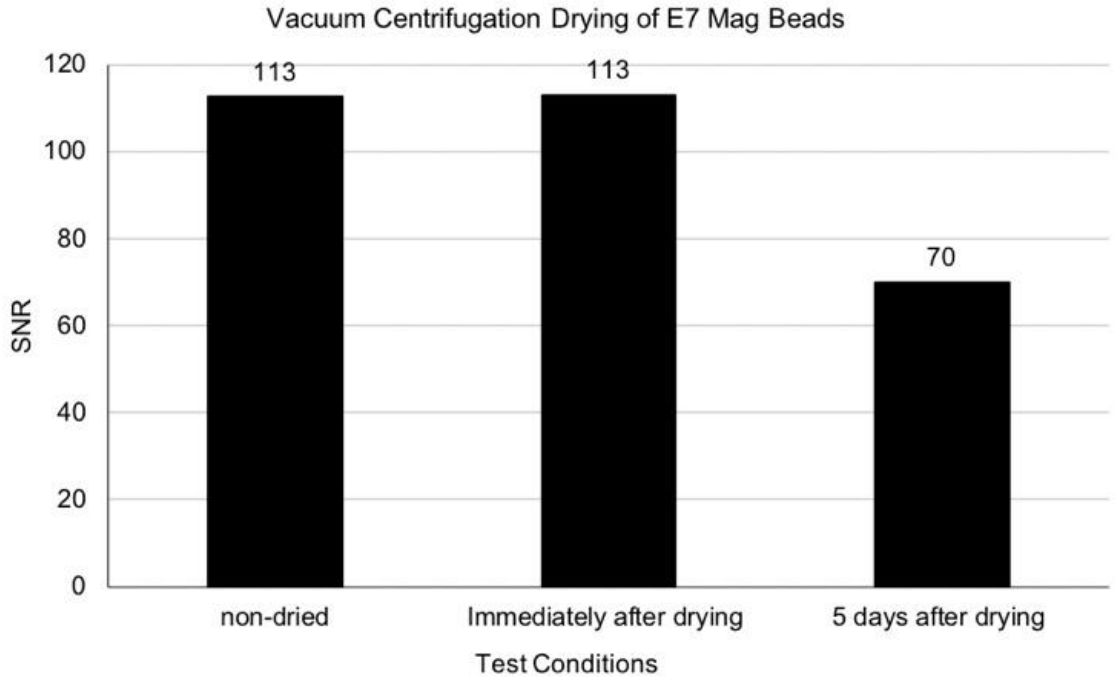

Figure 40: Immunoprecipitation assays were performed at set time points in order to determine E7 conjugated bead pellet stability. The immunoprecipitation assay used 10 uL of E7 conjugated beads, 200 ng/mL anti-E7 mouse monoclonal, and 1:500 anti-mouse Q-dot 655. Tests were performed on non-dried beads, immediately after drying, and 5 days after drying.

The E7 conjugated beads did not lose signal due to the vacuum centrifugation process, however the beads did not retain signal stability as expected. Immediately after the vacuum centrifugation process no loss of signal was seen in an immunoprecipitation

assay. Five days after vacuum centrifugation the E7 conjugated bead pellet was seen to have lost 38% of signal as compared to pre-vacuum centrifugation and same day pellet testing. Vacuum centrifugation was not a viable way to create stable dry protein conjugated bead pellets. Additionally, the vacuum centrifugation pelleted conjugated beads never became monodisperse once resuspended and remained in an aggregate pellet which is undesirable for compatibility with the microfluidic magnetic aperture.

Lyophilization

Lyophilization tests were conducted in order to create stable bead pellets. A mixture of 10 uL of either conjugated beads or unconjugated beads was created with 5 uL of 50% trehalose and 12.5 uL of 20% mannitol and left to lyophilize overnight. The total volume per pellet was 27.5 uL of bead sugar mix. The protein conjugated lyophilized beads had a honeycomb like crystallization shape while the unconjugated lyophilized beads had a smoothened crystallization shape.

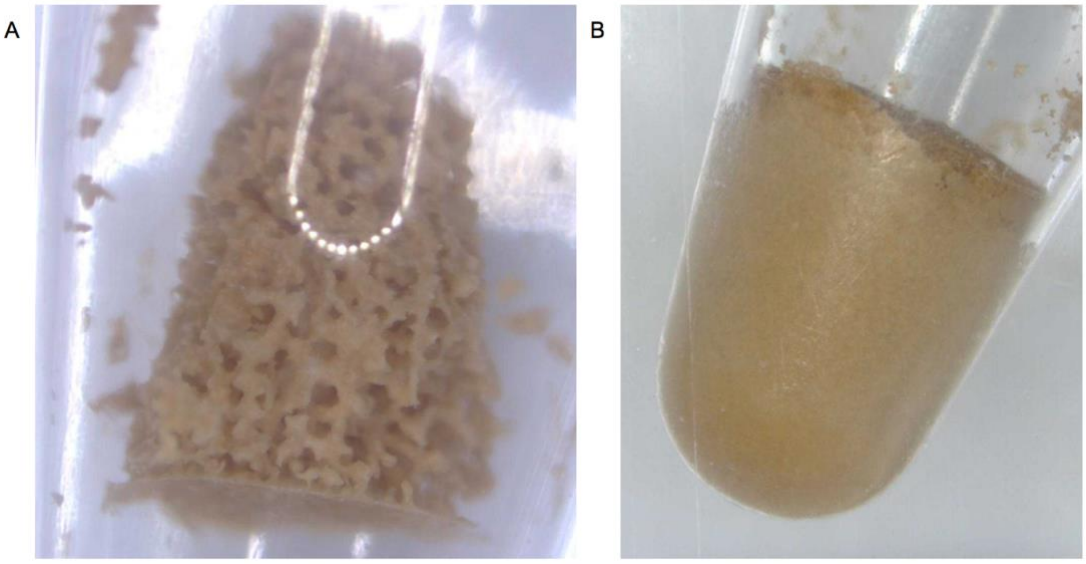

Figure 41: (A) Protein conjugated beads lyophilized pellet (B) Unconjugated beads lyophilized pellet. The pellets are in PCR tubes. The PCR tube has a volume of 0.2 mL, inner diameter of 5.5 mm, and height of 21.5 mm. The pellets are approximately 5 - 5.5 mm in length and 1.5 – 2 mm in width.

The lyophilized bead pellets had some static activity. When taking the lyophilized bead pellet out of the tube in which it was lyophilized some beads remain statically stuck to the plastic tube, and some will stick to whatever is used to remove the pellet from the tube, e.g., plastic tweezers, gloves.

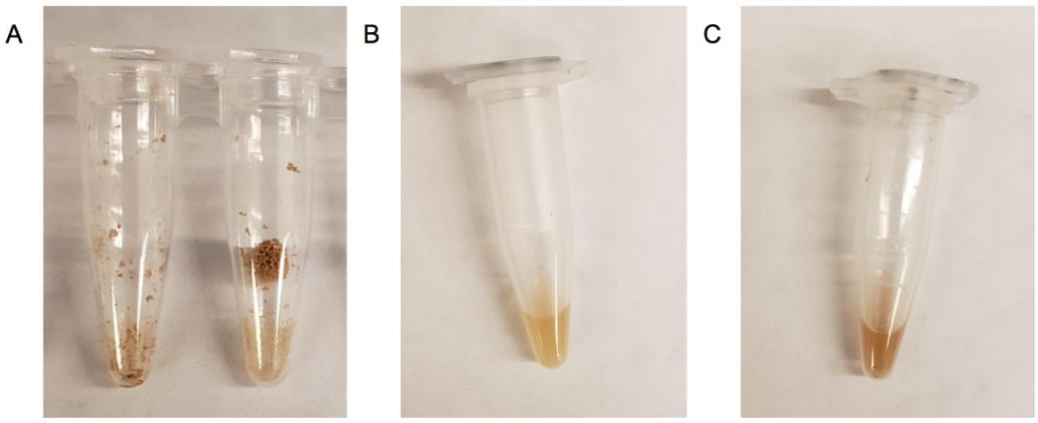

Figure 42: (A) Tube with protein conjugated bead pellet removed and tube with protein conjugated bead pellet (B) Lyophilized bead pellet resuspended in 0.1% PBST 0.1% BSA buffer. (C) Un-lyophilized beads suspended in 0.1% PBST 0.1% BSA buffer. The PCR tube (A) has a volume of 0.2 mL, inner diameter of 5.5 mm, and height of 21.5 mm. The Eppendorf tube (B and C) has a volume of 1.5 mL, inner diameter 8.0 mm, and height 39.0 mm

The bead loss through static interactions with plastic, the sugar mixture, or a combination of both did appear to dilute the concentration of the beads. The opacity of the buffer can be used to visually estimate the amount of beads that are in solution. The beads are a brown opaque color, so the darker the buffer the more beads are suspended in solution.

The lyophilized bead pellet did not interact with the magnetic aperture when in dry form. The lyophilized bead pellet can be placed in the microfluidic chip during construction of the microfluidic chip and sealed into the microfluidic chip without losing form. The 3 mm magnetic aperture can be attached to the microfluidic chip once the lyophilized bead pellet is sealed into the microfluidic chip and it will not exert strong enough magnetic forces to disform or pull the lyophilized bead pellet until the addition of

buffer and the lyophilized bead pellet is rehydrated. Upon rehydration by the addition of buffer the beads become monodisperse and are readily manipulated by the magnetic forces of the 3 mm magnetic aperture.

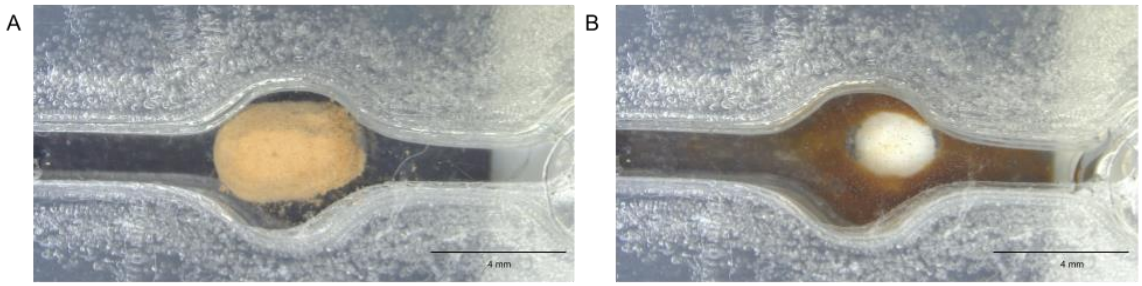

Figure 43: (A) Lyophilized bead pellet in microfluidic chip with 3 mm magnetic aperture before the addition of 0.1% PBST 0.1% BSA buffer. (B) Lyophilized bead pellet in the microfluidic chip with 3 mm magnetic aperture 1 minute after the addition of 0.1% PBST 0.1% BSA buffer. The scale marker line in the image represents 4 mm.

When the lyophilized bead pellet is resuspended in buffer the beads become monodisperse within solution. Upon the addition of buffer, the pellet is immediately rehydrated within 1 second of buffer addition. Some beads are lost to flow, but most remain around the magnetic aperture. The beads form around the magnetic aperture, leaving the space inside the magnetic aperture clear and ready for fluorescence reading in the point of care reader.

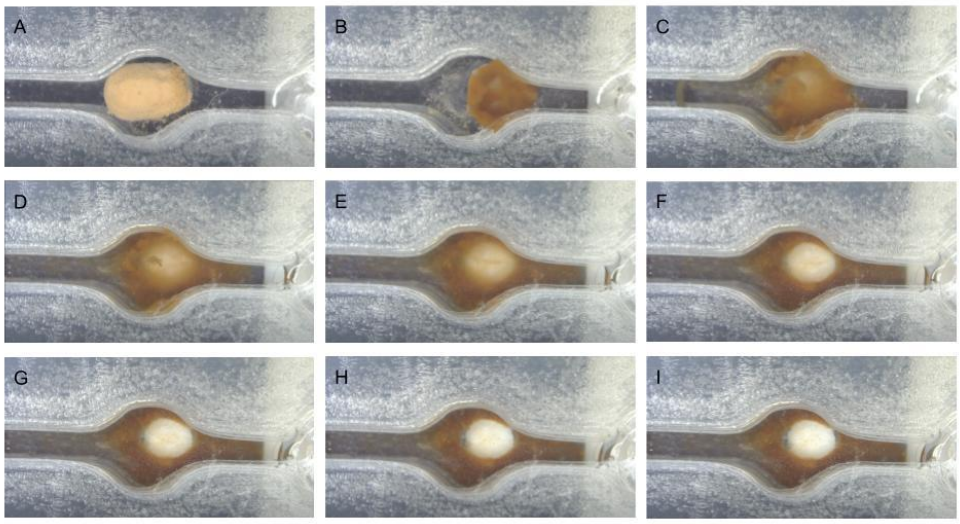

Figure 44: Photographs adapted from a video of the resuspension of the lyophilized bead pellet in 0.1% PBST 0.1% BSA buffer. (A) Before 0.1% PBST 0.1% BSA buffer (buffer) addition. (B) 1 second after buffer addition. (C) 2 seconds after buffer addition. (D) 5 seconds after buffer addition. (E) 10 seconds after buffer addition. (F) 20 seconds after buffer addition. (G) 30 seconds after buffer addition. (H) 45 seconds after buffer addition. (I) 1 minute after buffer addition. For scale see figure 43.

Lyophilization stability was tested through an immunoprecipitation assay performed at 5 days and 25 days post lyophilization. There was no significant loss of signal from immunoprecipitations performed with lyophilized beads at either time point.

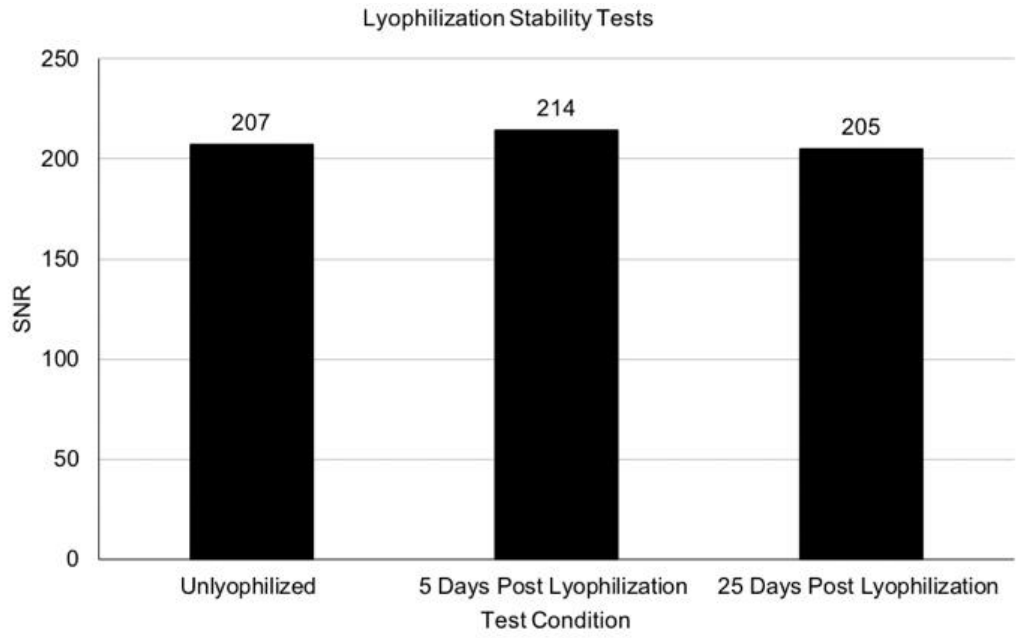

Figure 45: Immunoprecipitation assays were performed with anti-GST conjugated beads either lyophilized or lyophilized and conducted at different time points past lyophilization. The anti-GST conjugated beads were resuspended in 100 ul 0.1% PBST 0.1% BSA if lyophilized and were mixed with 1 ug (4uL) recombinant E7 protein and 1:100 (200 ng/mL) anti-E7 monoclonal for 20 minutes, they were given one wash step, and then mixed with 1:100 concentration of Alexa Fluor 488 anti-mouse in 0.1% PBST 0.1% BSA and given one wash before being read in the plate reader.

On Chip Assay

The complete indirect ELISA has been performed on chip. Ten microliters of E7 beads were assayed in the microfluidic chip and a protocol was established. The assay takes roughly 35 minutes from start to finish, though it is possible that this amount of time can be lessened through experimentation.

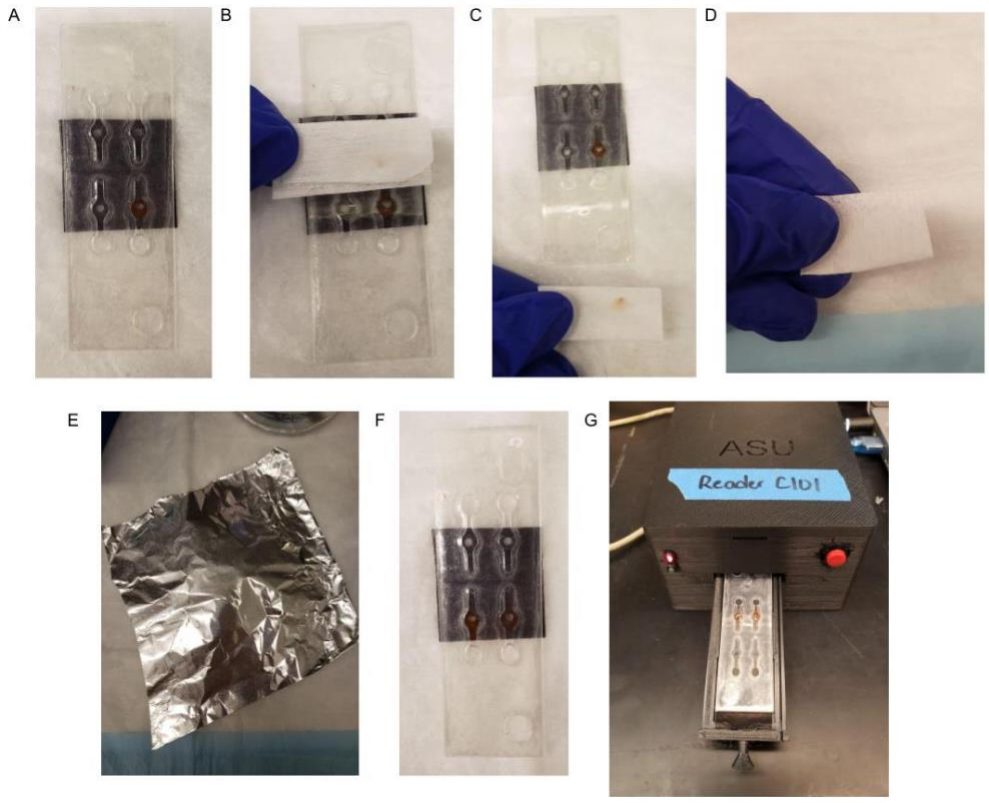

Figure 46: (A) 10 uL of E7 beads are resuspended in the chip with 15 uL of 0.1% PBST 0.1% BSA. (B) After incubation with anti-E7 monoclonal for 15 minutes an absorbent pad is used to absorb the buffer and primary mix through capillary action. (C) Some beads were lost to flow during the first addition of the absorbent pad to the chip. (D) The absorbent pad after the first wash step. No beads were lost to flow during this step, and no further beads were lost to flow in any additional steps after the first application of the absorbent pad. (E) Alexa Fluor 488 was added to the microfluidic chip and it was covered with aluminum foil to prevent photobleaching of the fluorophore. (F) The un-assayed beads were added to the microfluidic chip for reading of the bead background level. (G) The microfluidic chip inserted into the point of care reader for fluorescence detection. For microfluidic chip and magnetic strip dimensions see figure 2. The magnetic strip has a 3 mm aperture. For point of care reader dimensions see figure 1.

The on chip indirect ELISA showed promising results. The SNR of the assayed beads is in a range that is appropriate for point of care detection. The SNR was calculated by finding the slope of each sample, the assayed E7 beads, the un-assayed E7 beads, and the empty microfluidic chip. The slope of the empty microfluidic chip was subtracted from the slopes of the assayed E7 beads and the un-assayed E7 beads in order to account for the autofluorescence of the microfluidic chip. The SNR of the assayed beads was created by calculating the background adjusted slope of the assayed beads over

the background adjusted slope of the un-assayed beads. The SNR of the un-assayed beads was used as a marker of bead based background. The SNR of the un-assayed beads was created by calculating the raw slope of the un-assayed beads over the raw slope of the microfluidic chip. An SNR close to 1 means that the signal is indistinguishable over background, therefore the un-assayed beads do not have significant signal over the signal one might get from reading the empty microfluidic chip itself.

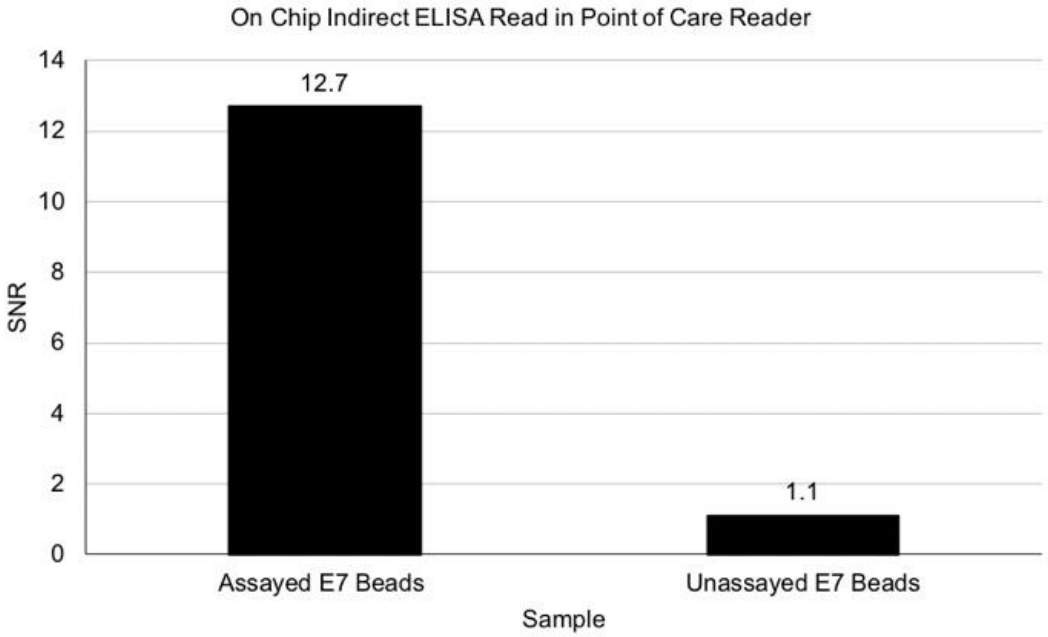

Figure 47: The assayed beads are 10 uL of E7 conjugated beads which were used in an on chip indirect ELISA assay. 10 uL of beads were resuspended in 15 uL of 0.1% PBST 0.1% BSA and 200 ng/mL anti-E7 monoclonal antibody. The chip was let to sit for 15 minutes. An absorbent pad was used to remove the primary monoclonal and buffer mix and then a wash step was performed with 20 uL of 0.1% PBST 0.1% BSA. An absorbent pad was used to remove the wash buffer and 20 uL of 1:100 Alexa Fluor 488 in 0.1% PBSTT 0.1% BSA was added to the chip. The chip was covered in foil and left to sit for 15 minutes. An absorbent pad was used to remove the secondary and buffer mix and a wash step was performed. A final removal of wash buffer and resuspension in 0.1% PBST 0.1% BSA was done and then the beads were read in the point of care reader. The un-assayed beads are beads that are E7 conjugated but did not undergo addition of monoclonal or secondary.

The on chip assay was tested with the indirect ELISA, sandwich ELISA, and NAPPA sandwich ELISA protocols. Anti-E7 monoclonal antibody was used as a predicted positive sample test and anti-EBV (Epstein–Barr virus nuclear antigen) monoclonal antibody was used as a negative control. The anti-EBV monoclonal antibody

was used a negative control because it should not bind to the E7 conjugated onto the beads in the indirect ELISA assay, or to the recombinant E7 or IVTT E7 added to the sandwich ELISA or NAPPA sandwich ELISA assays.

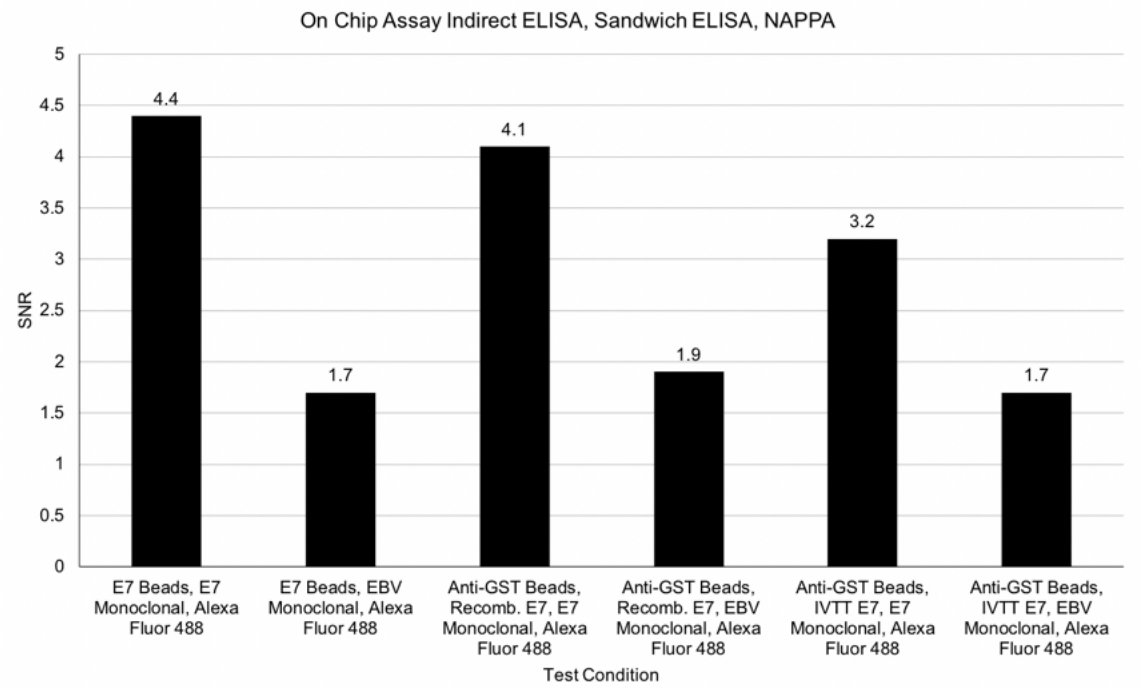

Figure 48: The beads used were 10 uL of E7 conjugated beads which were used in an on chip indirect ELISA assay, 20 uL of anti-GST beads which were used in an on chip sandwich ELISA assay and on chip NAPPA sandwich ELISA Assay. 10 uL of beads were resuspended in 15 uL of 0.1% PBST 0.1% BSA. The indirect ELISA resuspension was 200 ng/mL anti-E7 or anti-EBV monoclonal antibody. The sandwich ELISA and NAPPA sandwich ELISA resuspensions were 4 uL of recombinant E7 or IVTT E7, respectively, and 200 ng/mL anti-E7 or anti-EBV monoclonal antibody. The chip was let to sit for 15 minutes. An absorbent pad was used to remove the primary or pre-mix primary and protein resuspensions and then a wash step was performed with 20 uL of 0.1% PBST 0.1% BSA. An absorbent pad was used to remove the wash buffer and 20 uL of 1:100 Alexa Fluor 488 in 0.1% PBSTT 0.1% BSA was added to the chip. The chip was covered in foil and left to sit for 15 minutes. An absorbent pad was used to remove the secondary and buffer mix and a wash step was performed. A final removal of wash buffer and resuspension in 0.1% PBST 0.1% BSA was done and then the beads were read in the point of care reader.

The on chip assay is specific to E7, as a difference in signal is seen between the sample test analyte with E7 monoclonal and the negative control using EBV monoclonal. The signal overall for each assay type will need to be increased through methods to reduce background in the microfluidic assay and in the point of care reader system before adapting the assays to clinical plasma samples.

Table 4

Plate ELISA Comparison of EBV and E7 Monoclonal

Monoclonal and Protein	SNR
Anti EBV and EBV Protein	1993
Anti E7 and E7 protein	1489

A plate ELISA was completed with the EBV monoclonal to make sure that the difference seen in SNR in the on chip assay was not due to difference in the quality or capacity of the monoclonal antibodies to bind antigens. Both monoclonals have similar SNR and capture of their respective target antigens.

Cost Analysis

A key part of point of care assays is the creation of low cost devices. It is important for point of care diagnostics to have reduced costs in order for the assays to be accessible in low resource settings or developing nations. A cost analysis of the on chip assay was performed with both fluorophore options.

Table 5

Q-dot 655 Multiplexed Assay Components

Material	Cost	Amount Provided	Unit	Cost per one unit	Amount Used in Assay	Cost per Sample Test
Q-dot 655 Secondary	374	200 uL	uL	1.87	0.2	0.374
Carboxylic Acid Beads	174	2 mL	uL	0.087	40	3.48
Magnetic Sheet	12.99	Five 8" x 10" Sheets	sq in	2.598	0.0125	0.032475
Microfluidic Chip	5	n/a	n/a	n/a	n/a	5

Table 6

Alexa Fluor 488 Multiplexed Assay Components

Material	Cost	Amount Provided	Unit	Cost per one unit	Amount Used in Assay	Cost per Sample Test
Alexa Fluor 488 Secondary	221	1 mL	uL	0.221	1	0.221
Carboxylic Acid Beads	174	2 mL	uL	0.087	40	3.48
Magnetic Sheet	12.99	Five 8" x 10" Sheets	sq in	2.598	0.0125	0.032475
Microfluidic Chip	5	n/a	n/a	n/a	n/a	5

The individual components of the on chip assay were analyzed in order to calculate the cost of each component at the amounts that they were used in the assay. The highest cost for a single component is the microfluidic chip, but this does not account for any bulk discounts from manufacturers. If the assay were to be scaled up then there are high volume discounts available from the manufacturers of the materials utilized in the creation of the chip that could be utilized in order to decrease associated costs.

Table 7

Total Assay Costs

Assay	Assay Cost	Total Cost with Microfluidic Chip	Cost/Antigen (3 Antigens, 1 Control per Chip)
Q-dot 655 Multiplexed Assay	3.89	8.89	2.96
Alexa Fluor 488 Multiplexed Assay	3.73	8.73	2.91

The total cost of the assay per antigen was calculated and both fluorophores are around the same price, approximately $3 per antigen tested.

CHAPTER 4

DISCUSSION

Here it is demonstrated that a proof of concept microfluidic assay design for rapid detection of antibodies is amenable to fluorescence detection in point of care settings. The data demonstrates that the proof of concept microfluidic assay is rapid, low-cost, specific, and relevant to serology detection in point of care settings. The assay detects antibody responses to analytes with the point of care reader system and is realized in an on chip capacity. Additionally, the microfluidic system and detection elements, such as the point of care reader, are portable and the microfluidic chip and reagents are stable and readily transportable with the ability to lyophilize the magnetic beads and reagents, which is ideal for global health diagnostic assays where the system is intended to be sent to low resource areas and developing nations. With the integration of anti-GST capture antibodies conjugated to the magnetic beads in the microfluidic system, many analytes can be detected without large changes to the existing assay structure. This gives the ability to adapt the system to analytes of interest rapidly, especially when paired with the NAPPA technology of plasmid based cell free protein expression.

This project displays a proof of concept for a magnetic microfluidic based ELISA but is limited in the fact that further experimentation is necessary with clinical samples before widespread comparisons can be made with current art. Comparisons with current art are made on assay structure and feasibility rather than sensitivity and specificity, as those metrics must be compared based on data from clinical plasma samples, as they are in the current art. The magnetic microfluidic system aligns well with other current systems in microfluidic technology. Fan et al. describe a multiplexed microfluidic system

that utilizes a PDMS chip bound to a glass slide printed with DNA-antibody conjugates for protein biomarker capture and enables on chip blood separation of a finger prick sample. Their multiplexed system utilized fluorescence detection and the on chip assay was approximately 10 minutes. They were able to provide a proof of principle for use of the microfluidic technology to create cancer patient profiles based on cancer biomarkers, cytokines, and functional proteins involved in the complement system and other immune functions that were detected in plasma (2008). Zhao et al. describe a magnetic bead based microfluidic assay on a PDMS chip bound to a glass slide that utilized fluorescence detection. Their system utilized antibody conjugated magnetic beads to detect plasma exosomes derived from ovarian tumors. Their system required 20 uL of plasma for analysis and was a 40 minute process (2017). Gao et al. describes a magnetic beads based microfluidic system that utilizes antibody conjugated magnetic beads and gold nanoparticles for detection. They use a surface-enhanced Raman scattering (SERS)-based solenoid-embedded microfluidic device to detect anthrax biomarkers (2015). This magnetic bead based microfluidic system follows closely in line to current systems in the capacity for multiplexing, rapid assay time, sample and reagent volumes, and quantitative results through fluorescence detection.

One challenge that was identified in this system was with bead retention. Under flow conditions, either during lyophilization resuspension or during initial flow and wash steps of the on chip assay protocol, there is a small amount of beads that are lost to flow. This problem could be solved by utilizing higher gauss magnetic sheets for the apertures. Currently the magnetic sheets used for the magnetic apertures have a gauss level of 350, which is sufficient to hold most of the beads. During the on chip assay, beads were only

lost to flow during the first use of the absorbent pad. This may indicate that there is an excess of beads than the magnet can hold via magnetic attraction when using 10 uL of beads in the assay, and the beads that the magnet is not attracting are lost to initial flow from the strength of the capillary action mechanism of the absorbent pad. The fact that no further wash steps draw beads via flow with use of the absorbent pad gives further evidence that this might be the case. An additional way to solve the problem of bead retention could be to utilize two magnetic apertures, one adhered to the bottom of the chip and one adhered to the top. The use of two apertures would need to be evaluated to determine the effect it would have measurements in the read frame in the point of care reader. Additionally, it would complicate construction of the microfluidic chip, as it would be best to have the apertures perfectly aligned, which may be difficult when creating the microfluidic chips by hand.

Another challenge that was identified was the autofluorescence of the plastics used in the microfluidic chip. Apertures were created to reduce the impact of autofluorescence on the reading of samples, however, the apertures placement in the read frame may still obstruct signal and reduce detection levels. Additionally, the magnetic beads opacity may also obstruct signal in the read frame, which was another challenge the apertures attempt to resolve. It may be possible to overcome the challenges of obstruction within the read frame from the magnetic apparatuses by utilizing clear magnetics, if they were to become commercially available. Kobayashi et al. describe an optically transparent magnet made from FeCo-(Al-fluoride) nanogranular films. The films they utilize have a nanocomposite structure that incorporates nanometer sized

ferromagnetic granules dispersed in an Al-fluoride crystallized matrix, which allows for high optical transparency in the visual light region (2016).

The indirect ELISA, sandwich ELISA, and NAPPA sandwich ELISA assays on chip could be tested in a non-magnetic capacity. Traditional ELISAs are performed by passive binding of proteins and antibodies to polystyrene plates. Protein and antibodies bind to plastic through hydrophobic and hydrophilic interactions between the plastic and any non-polar residues on the proteins. In most passive binding applications, the wells are over saturated with an excess of protein suspended in an alkaline buffer, such as carbonate-bicarbonate (Advansta Inc., 2015). The passive binding capacity of the molecules depends on the hydrophobicity or hydrophilicity of both the plastic and the biomolecules. Antibodies and water soluble proteins bind well through hydrophilic interactions, thus plates used for immunoassays are typically optimized to utilize these hydrophilic interactions for passive binding (Thermo Fisher Scientific, 2017). Polystyrene is a long carbon chain that has benzene rings on every other carbon and is by nature hydrophobic. It is typically treated radioactively to modify the surface to be hydrophilic through the addition of carboxylic acid on the carbons accessible from the broken benzene rings (Gibbs et al., 2017). The microfluidic chip is made from polyethylene terephthalate (PET), which is a linkage between terephthalates and ethylene through esterification reaction between terephthalic acid and ethylene glycol or trans-esterification reaction between ethylene glycol and dimethyl terephthalate (Zare, 2017; Omnexus, 2017). PET, like polystyrene, is by nature hydrophobic but it can be adapted to become more hydrophilic though chemical or radiation treatments (Gotoh et al., 2011). The microfluidic chip as it is now is not well suited to bind proteins or antibodies to the

well surface, but if the plastic is pre-treated it may be possible to utilize the chip in a way similar to the polystyrene plates utilized in traditional ELISAs. Additionally, it is possible that proteins or antibodies could bind to the rough edges of the microfluidic chip well or to any exposed pressure sensitive adhesive at the edges of the well, which may minimize the need to pre-treat the PET for passive binding applications.

While the microfluidic magnetic system was utilized for serology assays in this project, it has wider implications and is amenable to other types of protein assays. For example, the antibody conjugated magnetic bead based microfluidic design could be adapted to protein immunoprecipitation or quantification in small volume complex samples. Previous preliminary experiments showed that elution of antibodies off of the beads and quantification of capture secondary is viable using Pierce Gentle AG/AB Elution Buffer and Alexa Fluor 488 conjugated secondary. The magnetic microfluidic system is versatile and can be adapted further to fit the needs of additional experimental applications.

CHAPTER 5

FUTURE DIRECTIONS

On Chip Assay Modifications

The on chip assay will need to be modified in order to reduce background in the assay. The background could be caused by many variables, it could be caused by the beads causing diffraction or light scattering in the read frame, or the beads dispersing too far from the read frame in the edges of the magnetic aperture, or by non-optimal primary and secondary antibody concentrations. Preliminary modifications to the apertures were made to see if it was feasible to change the aperture and still have bead retention. Two sizes of ring shaped apertures were tested with beads under flow. The smaller diameter aperture worked best at keeping the beads centered closely to the aperture and retained the beads better. The smaller ring shaped aperture is a viable solution to bead dispersal causing signal dampening and can be adapted for use in future versions of the on chip assay.

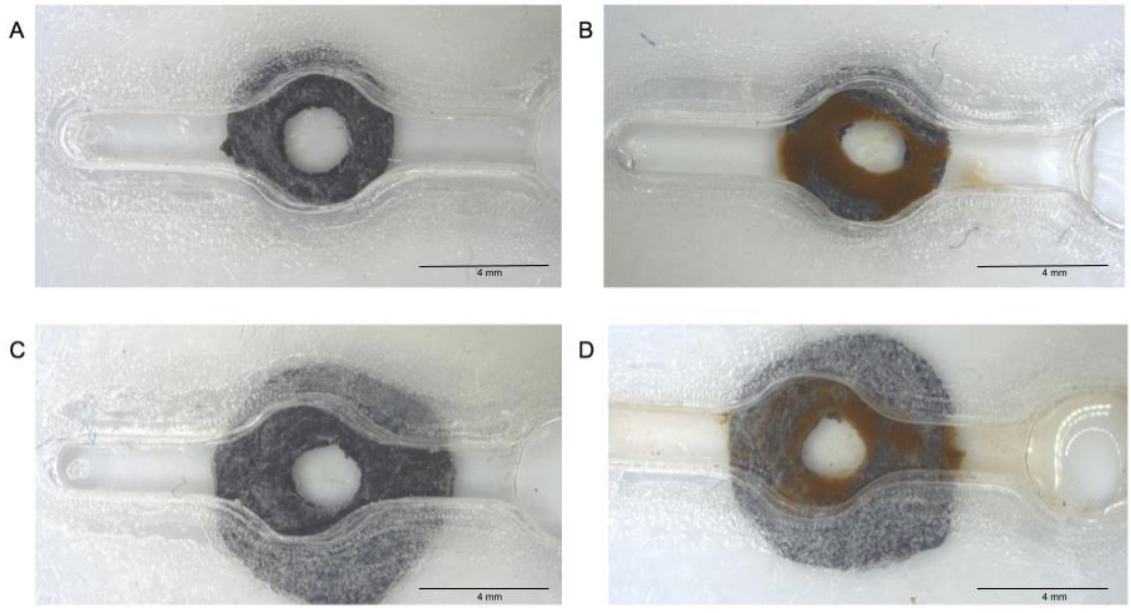

Figure 49: (A) The smaller ring shaped aperture on the microfluidic chip. (B) The smaller ring shaped aperture with beads after simulated flow conditions. (C) The larger ring shaped aperture on the microfluidic chip. (D) The larger ring shaped aperture with beads after simulated flow conditions. The scale marker line in the image represents 4 mm.

Preliminary tests were done regarding interference from the beads themselves, Alexa Fluor 488 was used to see if elution of the complex off of the beads is a viable option.

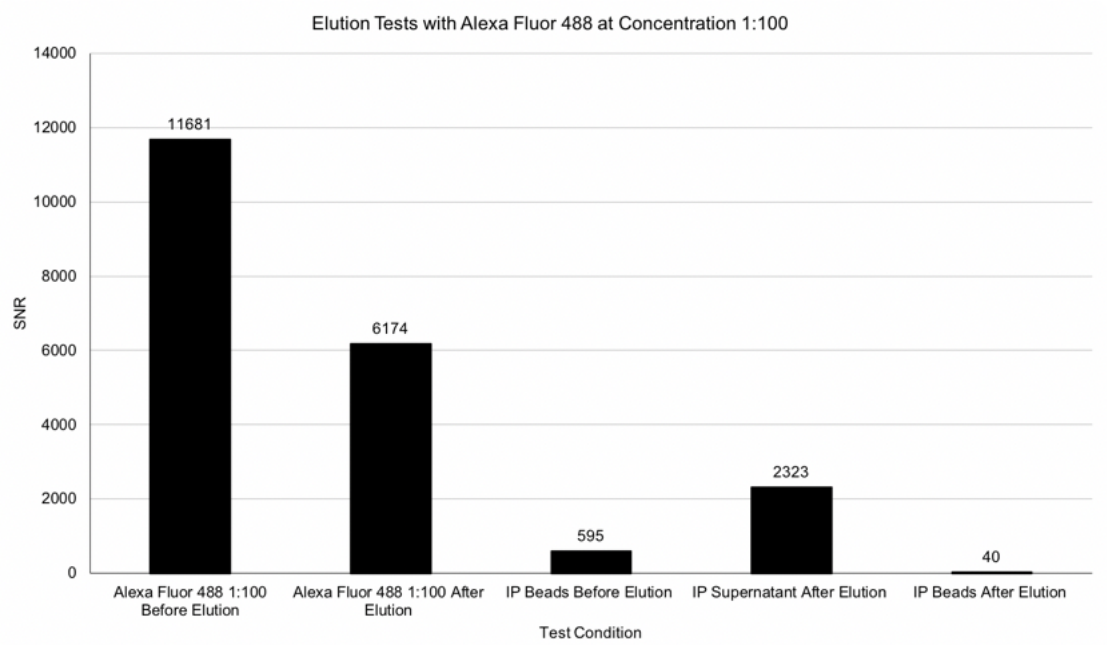

Figure 50: Alexa Fluor 488 at a 1:100 concentration is compared suspended in PBS buffer and suspended in elution buffer. Alexa Fluor 488 was used in an immunoprecipitation assay at 1:100 concentration with 10 uL of E7 conjugated magnetic beads and 200 ng/mL anti-E7 monoclonal. The results of the beads that have been used in the assay are shown, then the results of the supernatant after a 10 minute elution step with the elution buffer was performed on the beads, then the results of the beads after the fluorophore has been eluted are shown.

The results show that elution is a viable application for the assay using the Alexa Fluor 488 fluorophore. While it appears that the beads cause significant signal dampening it must be noted that these preliminary experiments were read in the plate reader, where the beads are in the laser line directly. It cannot be directly applied to the microfluidic and point of care reader system where the beads are held outside of the laser line. Experiments must be conducted further with elution in the on chip system, but eluting the

fluorescent signal off of the bead may be a viable solution to reducing the background. A microfluidic chip has already been created by the Blain Christen laboratory that can be adapted to an elution based microfluidic assay.

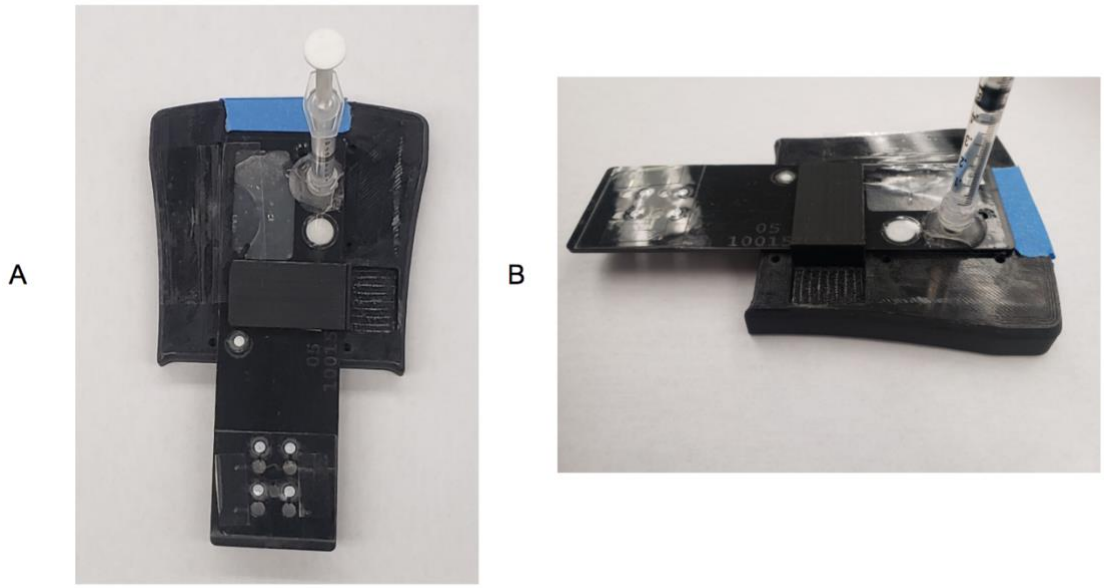

Figure 51: The microfluidic chip that can be adapted for an elution based on chip microfluidic assay. (A) Top view. (B) Side view. The chip is 36 mm wide and 122 mm long.

The chip shown above is created to utilize channels that can be opened and closed based on the positioning of a blocking mechanism. The chip utilizes positive pressure flow via a syringe rather than capillary flow as in the current on chip assay. The channels lead either to a waste reservoir or to wells that are read in the point of care reader system. If the microfluidic assay were to be adapted to this chip ideally the magnetic beads would be secured with a magnet in the area below the syringe, the channels leading to the read wells would be blocked off while the assay is being performed, sending the output to the waste reservoir. When it is time for the final elution step the channels to the read wells will be opened while the channels to the waste reservoir will be blocked, sending the eluted signal to the read wells.

Blocking Buffer Optimizations

In order for the assay to be applied to human diagnostics it will need to undergo blocking buffer optimizations. Human sera is ‘sticky’, meaning that it will bind to open unbound space on the magnetic beads (Güven et al., 2014). Treating the beads with a blocking buffer before addition of the primary will cause the unbound surface to be bound by the non-reactive protein in the blocking buffer rather than the plasma and will also stabilize already bound proteins. This will reduce background in the assay and increase the signal to noise ratios. Common protein blocking buffers are bovine serum albumin (BSA) or non-fat dry milk. Protein blocking buffers adhere permanently, and the concentration must be optimized experimentally to determine the concentration where the background interactions are blocked but the wanted binding interactions are not blocked. Tween-20 is a common detergent blocking buffer and is typically used at concentrations 0.1 - 0.01%. Detergent blocking buffers are not permanent and are typically used in conjunction with protein blocking buffers to enhance blocking (Advansta Inc., 2015). Experimental findings with human plasma have found that there is unbound space on the magnetic beads that is binding plasma and causing increased levels of background, and this will need to be addressed before application of the assay to clinical plasma samples.

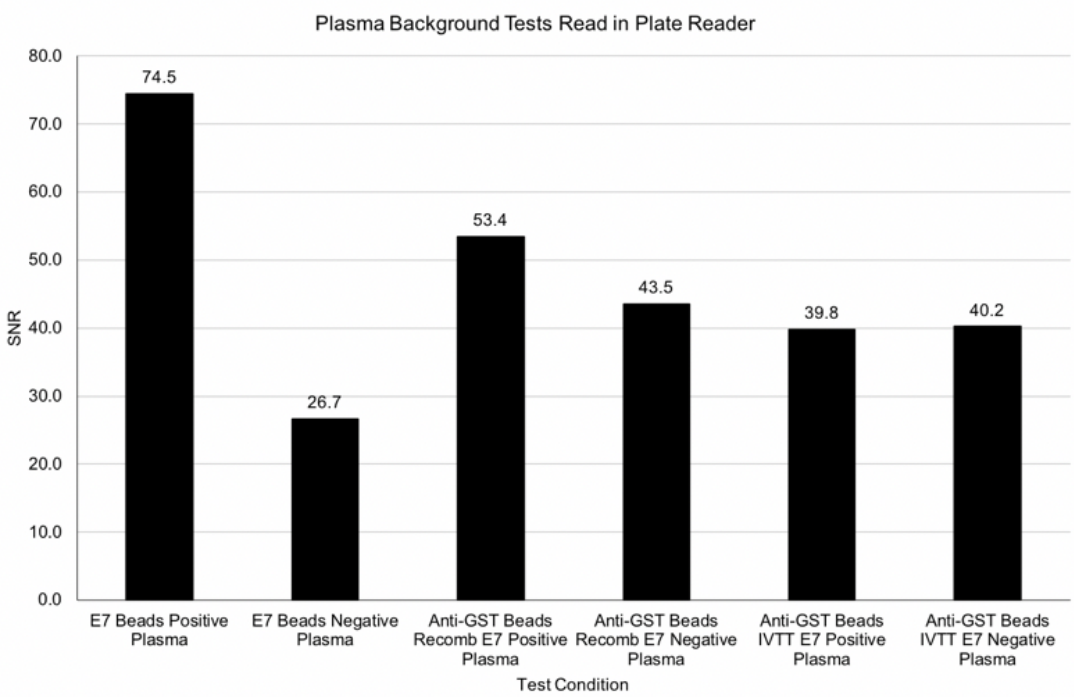

Figure 52: An immunoprecipitation reaction was carried out with test conditions using 10 uL of E7 conjugated beads or anti-GST conjugated beads. One test condition utilized 10 uL of E7 conjugated beads per test. The beads were mixed with 1 uL of positive plasma or 1 uL of negative plasma for 20 minutes, were given one wash step, and were then mixed with Q-dot 655 at a 1:500 dilution in 0.1% PBST 0.1% BSA for 20 minutes and given one final wash before being read in the plate reader. Another test condition utilized 10 uL of anti-GST conjugated beads per test. The beads were mixed with 1 uL of positive plasma or 1 uL of negative plasma and 1 ug (4 uL) of recombinant E7 protein for 20 minutes, were given one wash step, and were then mixed with Alexa Fluor 488 at a 1:100 dilution in 0.1% PBST 0.1% BSA for 20 minutes and given one final wash before being read in the plate reader. The last test condition utilized 10 uL of anti-GST conjugated beads per test. The beads were mixed with 1 uL of positive plasma or 1 uL of negative plasma and IVTT E7 protein at a concentration of 1:25 (4 uL) for 20 minutes, were given one wash step, and were then mixed with Alexa Fluor 488 at a 1:100 dilution in in 0.1% PBST 0.1% BSA for 20 minutes and given one final wash before being read in the plate reader.

The E7 beads showed less background due to plasma than the anti-GST beads. This may be due to the direct conjugation of protein to bead and direct binding of primary antibody to bead, versus the stacking interaction of conjugated anti-GST, and the addition of protein and sera pre-mixed. The above figure represents the SNR of the positive and negative samples, but a background adjusted SNR can be created by calculating the positive plasma SNR over the negative plasma SNR.

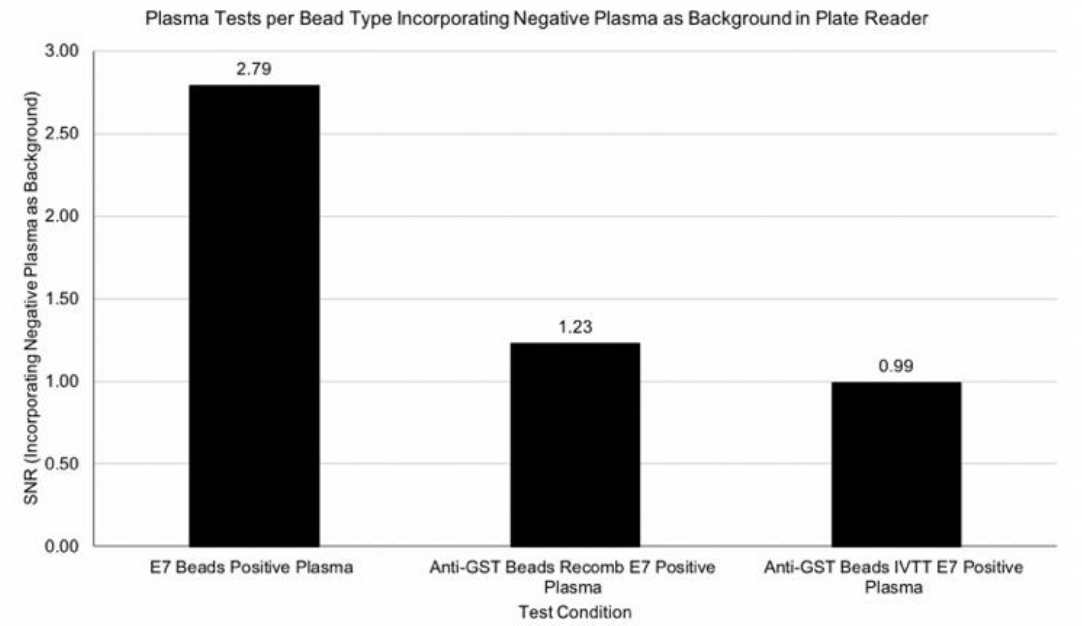

Figure 53: This figure details the true background of the samples read in figure #. The positive plasma was compared over the negative plasma to give the true SNR incorporating background for each test condition.

The background adjusted SNRs show that the background is very high, which lowers the SNR considerably. To rectify this, the magnetic beads will need to be blocked with either a higher concentration of bovine serum albumin (BSA) or with non-fat dry milk before addition of the primary antibody. A suggested experiment would be to test 1%, 2%, and 3% BSA in 0.1% PBST as well as 3% and 5% milk in 0.1% PBST with 10 ul of each bead type, E7 conjugated beads, anti-GST conjugated beads with recombinant E7 protein, and anti-GST beads with IVTT E7 protein, and positive and negative plasma. This test will determine the optimum blocking buffer at the optimum concentration. For incorporating the optimized blocking buffer to the final assay the beads should be resuspended in the chosen blocking buffer before addition of the plasma.

Biomarker Tests

The microfluidic system for indirect ELISA can be multiplexed to measure various biomarkers. Future adaptations of the assay can involve testing CTAG1, CTAG2,

and P53 as multiplexed markers for ovarian cancer, as well as testing E6, E7, E2, and E4 as multiplexed markers for HPV infection.

On Chip Microfluidic IVTT Expression

One capability of the point of care reader that was not utilized in this project is a heating element. A possible application of this project would be to utilize the heating element of the POC reader to express IVTT proteins within the microfluidic chip, simplifying the assay and removing the need to express the proteins outside of the system. It is possible to conjugate oligonucleotides to the MyOne Carboxylic Acid Dynabeads, and a protocol is outlined in the product manual from Invitrogen Life Technologies. By conjugating the pANT7_cGST plasmid to the magnetic beads, the IVTT proteins can be expressed within the chip. The necessary reagents, i.e., HeLa lysate, accessory proteins, and reaction mix, could be added to the chip and the POC reader could heat the mixture at 30 degrees Celsius for 90 minutes, thus performing the IVTT reaction. The assay would then commence as outlined in this project with the addition of primary and secondary antibodies. This would be beneficial in point of care applications where clinical use of the assay might not occur in spaces with a lab environment. It also reduces the need to transport or store pre-made IVTT proteins for use in the assay.

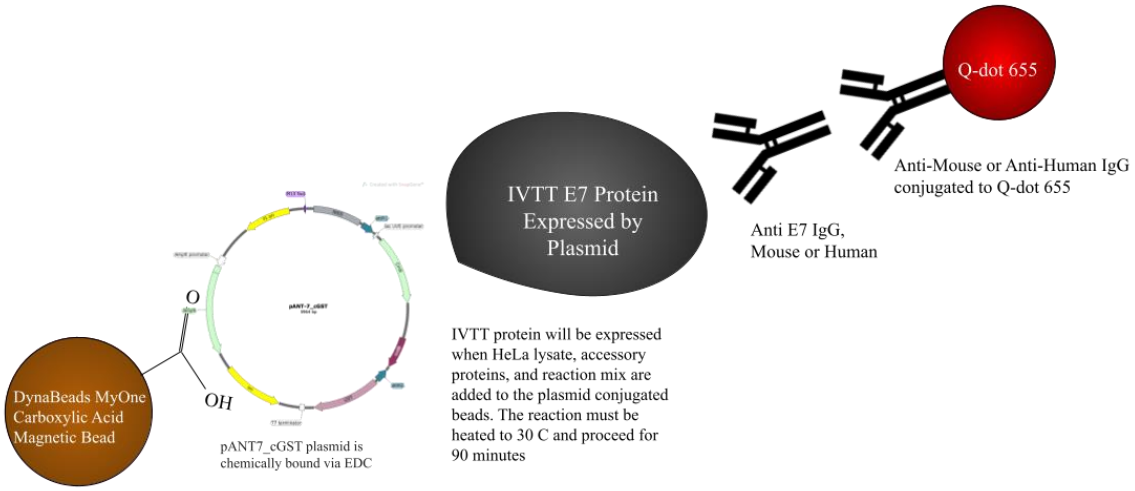

Figure 54: A diagram of the plasmid conjugated bead NAPPA indirect ELISA capture complex.

Dual IgM and IgG Detection

The narrow excitation and emission ranges of the Q-dots allows for the use of two or more secondary antibodies within the same assay. One potential application of this project would be to utilize two different Q-dot fluorophores for the detection of both IgM and IgG in a single assay. Dual detection of IgG and IgM would be beneficial in the context of HPV serology detection because it has been shown that during the immune response to HPV, the presence of IgM is indicative of an acute or current exposure to HPV while IgG is a reliable marker of past HPV exposure (Kerishnan et al., 2016). A combination of Q-dots that could be implemented are Q-dot 655 and Q-dot 800. These fluorophores have the same excitation wavelength but have different emission wavelengths. The POC reader could be equipped with a filter that would excite both fluorophores and based on the emission output IgM and IgG responses within the plasma could be differentiated.

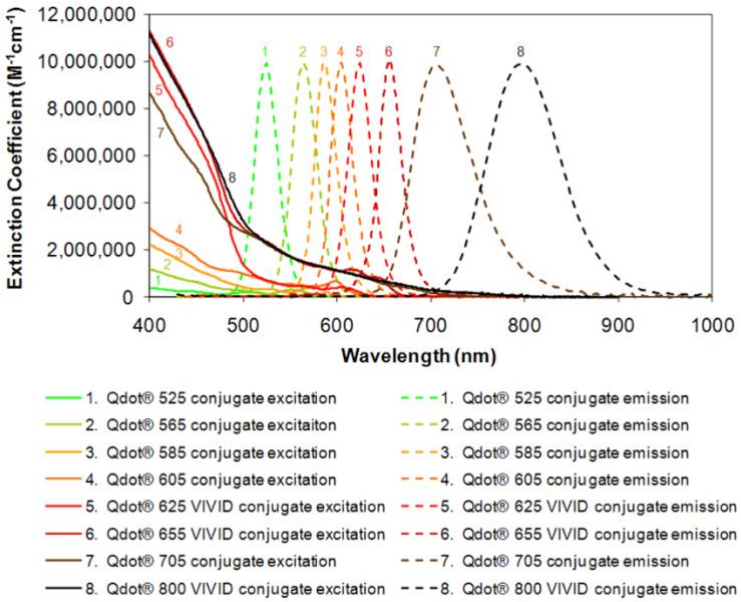

Figure 55: Figure 2 of the Invitrogen Molecular Probes Q-dot Secondary Antibody Conjugates product manual depicting the Q-dot excitation and emission wavelengths.

REFERENCES

Abdulkarim, B., Sabri, S., Deutsch, E., Chagraoui, H., Maggiorella, L., Thierry, J., Eschwege, F., Vainchenker, W., Chouaïb, S., & Bourhis, J. (2002). Antiviral agent Cidofovir restores p53 function and enhances the radiosensitivity in HPV-associated cancers. *Oncogene*, *21*(15), 2334–2346. https://doi.org/10.1038/sj.onc.1205006

Advansta Inc. (2015). *Enzyme-linked immunosorbent assays (ELISA)*. Advansta Wiki. Retrieved from https://advansta.com/wikis/enzyme-linked-immunosorbent-assays/

Anderson, K. S., Gerber, J. E., D'Souza, G., Pai, S. I., Cheng, J. N., Alam, R., Kesiraju, S., Chowell, D., Gross, N. D., Haddad, R., Gillison, M. L., & Posner, M. (2015). Biologic predictors of serologic responses to HPV in oropharyngeal cancer: The Hotspot Study. *Oral Oncology*, *51*(8), 751–758. https://doi.org/10.1016/j.oraloncology.2015.05.007

ASU Biodesign Institute. (2015, July 7). *Nappa technology*. Research Center Personalized Diagnostics. Retrieved from https://biodesign.asu.edu/personalized-diagnostics/nappa-technology

Bergot, A.-S., Kassianos, A., Frazer, I. H., & Mittal, D. (2011). New Approaches to Immunotherapy for HPV Associated Cancers. *Cancers*, *3*(3), 3461–3495. https://doi.org/10.3390/cancers3033461

Bharadwaj, M., Hussain, S., Nasare, V., & Das, B. C. (2009). HPV & HPV vaccination: Issues in developing countries. *The Indian Journal of Medical Research*, *130*(3), 327–333.

Black, E., & Richmond, R. (2018). Prevention of Cervical Cancer in Sub-Saharan Africa: The Advantages and Challenges of HPV Vaccination. *Vaccines*, *6*(3), 61. https://doi.org/10.3390/vaccines6030061

Boston University. (2013). Fluorochromes Brightness Chart from Boston University Flow Cytometry Core Facility. Boston.

Braaten, K. P., & Laufer, M. R. (2008). Human Papillomavirus (HPV), HPV-Related Disease, and the HPV Vaccine. *Reviews in Obstetrics and Gynecology*, *1*(1), 2–10.

Burd, E. M. (2003). Human Papillomavirus and Cervical Cancer. *Clinical Microbiology Reviews*, *16*(1), 1–17. https://doi.org/10.1128/CMR.16.1.1-17.2003

Centers for Disease Control and Prevention. (2012). *Human papillomavirus–associated cancers - united states, 2004–2008*. Centers for Disease Control and Prevention. Retrieved from https://www.cdc.gov/mmwr/preview/mmwrhtml/mm6115a2.htm.

Crosbie, E. J., Einstein, M. H., Franceschi, S., & Kitchener, H. C. (2013). Human papillomavirus and cervical cancer. *The Lancet*, *382*(9895), 889–899. https://doi.org/10.1016/S0140-6736(13)60022-7

Cusabio Technology. (2018, July 3). *Four types of Elisa*. CUSABIO. Retrieved from https://www.cusabio.com/c-20659.html

Dasari, S., Wudayagiri, R., & Valluru, L. (2015). Cervical cancer: Biomarkers for diagnosis and treatment. *Clinica Chimica Acta*, *445*, 7–11. https://doi.org/10.1016/j.cca.2015.03.005

De Freitas, A. C., Coimbra, E. C., & Leitão, M. da C. G. (2014). Molecular targets of HPV oncoproteins: Potential biomarkers for cervical carcinogenesis. *Biochimica et Biophysica Acta (BBA) - Reviews on Cancer*, *1845*(2), 91–103. https://doi.org/10.1016/j.bbcan.2013.12.004

Fan, R., Vermesh, O., Srivastava, A., Yen, B. K., Qin, L., Ahmad, H., Kwong, G. A., Liu, C.-C., Gould, J., Hood, L., & Heath, J. R. (2008). Integrated barcode chips for rapid, multiplexed analysis of proteins in microliter quantities of blood. *Nature Biotechnology*, *26*(12), 1373–1378. https://doi.org/10.1038/nbt.1507

Fish, K. N., & Davidson, M. W. (2009). Fluorescent biomarkers in neurons. *Encyclopedia of Neuroscience*, 261–271. https://doi.org/10.1016/b978-008045046-9.02003-9

Gao, R., Ko, J., Cha, K., Ho Jeon, J., Rhie, G.-eun, Choi, J., deMello, A. J., & Choo, J. (2015). Fast and sensitive detection of an anthrax biomarker using SERS-based solenoid microfluidic sensor. *Biosensors and Bioelectronics*, *72*, 230–236. https://doi.org/10.1016/j.bios.2015.05.005

Gibbs, J., Vessels, M., & Rothenberg, M. (2017). Immobilization Principles – Selecting the Surface for ELISA Assays: Application Note. Retrieved from https://www.corning.com/catalog/cls/documents/application-notes/CLS-DD-AN-454.pdf

Gotoh, K., Yasukawa, A., & Kobayashi, Y. (2011). Wettability characteristics of poly(ethylene terephthalate) films treated by atmospheric pressure plasma and ultraviolet excimer light. *Polymer Journal*, *43*(6), 545–551. https://doi.org/10.1038/pj.2011.20

Güven, E., Duus, K., Lydolph, M. C., Jørgensen, C. S., Laursen, I., & Houen, G. (2014). Non-specific binding in solid phase immunoassays for autoantibodies correlates with inflammation markers. *Journal of Immunological Methods*, *403*(1-2), 26–36. https://doi.org/10.1016/j.jim.2013.11.014

Harries, J., Moodley, J., Barone, M. A., Mall, S., & Sinanovic, E. (2009). Preparing for HPV vaccination in South Africa: Key challenges and opinions. *Vaccine*, *27*(1), 38–44. https://doi.org/10.1016/j.vaccine.2008.10.033

Hou, C.-W., Zhu, M., Anderson, K. S., Obahiagbon, U., & Christen, J. B. (2018). Assay development and storage for fluorescence-based lateral flow immunoassay. *2018 IEEE Life Sciences Conference (LSC)*. https://doi.org/10.1109/lsc.2018.8572244

Invitrogen. (2011). Qdot® Secondary Antibody Conjugates: User Guide. Retrieved from https://tools.thermofisher.com/content/sfs/manuals/mp11001.pdf

Jensen, A. B., Hubálek, F., Stidsen, C. E., Johansson, E., Öberg, F. K., Skjøt, M., & Kjeldsen, T. (2021). Cell free protein synthesis versus yeast expression – a comparison using insulin as a model protein. *Protein Expression and Purification*, *186*, 105910. https://doi.org/10.1016/j.pep.2021.105910

Jemal, A., Simard, E. P., Dorell, C., Noone, A.-M., Markowitz, L. E., Kohler, B., Eheman, C., Saraiya, M., Bandi, P., Saslow, D., Cronin, K. A., Watson, M., Schiffman, M., Henley, S. J., Schymura, M. J., Anderson, R. N., Yankey, D., & Edwards, B. K. (2013). Annual Report to the Nation on the Status of Cancer, 1975–2009, Featuring the Burden and Trends in Human Papillomavirus (HPV)–Associated Cancers and HPV Vaccination Coverage Levels. *JNCI: Journal of the National Cancer Institute*, *105*(3), 175–201. https://doi.org/10.1093/jnci/djs491

Kaarthigeyan, K. (2012). Cervical cancer in India and HPV vaccination. *Indian Journal of Medical and Paediatric Oncology: Official Journal of Indian Society of Medical & Paediatric Oncology*, *33*(1), 7–12. https://doi.org/10.4103/0971-5851.96961

Kerishnan, J. P., Gopinath, S. C. B., Kai, S. B., Tang, T.-H., Ng, H. L.-C., Rahman, Z. A., Hashim, U., & Chen, Y. (2016). Detection of human papillomavirus 16-specific IGG and IGM antibodies in patient sera: A potential indicator of oral squamous cell carcinoma risk factor. *International Journal of Medical Sciences*, *13*(6), 424–431. https://doi.org/10.7150/ijms.14475

Kobayashi, N., Masumoto, H., Takahashi, S., & Maekawa, S. (2016). Optically transparent ferromagnetic Nanogranular films with tunable transmittance. *Scientific Reports*, *6*(1). https://doi.org/10.1038/srep34227

Koczula, K. M., & Gallotta, A. (2016). Lateral flow assays. *Essays in Biochemistry*, *60*(1), 111–120. https://doi.org/10.1042/ebc20150012

Lee, C., Noh, J., O'Neal, S. E., Gonzalez, A. E., Garcia, H. H., & Handali, S. (2019). Feasibility of a point-of-care test based on quantum dots with a mobile phone reader for detection of antibody responses. *PLOS Neglected Tropical Diseases, 13*(10). https://doi.org/10.1371/journal.pntd.0007746

Miersch, S., & LaBaer, J. (2011). Nucleic acid programmable protein arrays: Versatile tools for array-based functional protein studies. *Current Protocols in Protein Science, 64*(1). https://doi.org/10.1002/0471140864.ps2702s64

Montgomery, M. P., Dune, T., Shetty, P. K., & Shetty, A. K. (2015). Knowledge and Acceptability of Human Papillomavirus Vaccination and Cervical Cancer Screening among Women in Karnataka, India. *Journal of Cancer Education, 30*(1), 130–137. https://doi.org/10.1007/s13187-014-0745-4

Munger, K., Gwin, T. K., & McLaughlin-Drubin, M. (2013). P16 in HPV-associated cancers. *Oncotarget, 4*(11), 1864–1865.

Ngoma, M., & Autier, P. (2019). Cancer prevention: Cervical cancer. *Ecancermedicalscience, 13*, 952. https://doi.org/10.3332/ecancer.2019.952

Obahiagbon, U., Smith, J. T., Zhu, M., Katchman, B. A., Arafa, H., Anderson, K. S., & Blain Christen, J. M. (2018). A compact, low-cost, quantitative and multiplexed fluorescence detection platform for point-of-care applications. *Biosensors and Bioelectronics, 117*, 153–160. https://doi.org/10.1016/j.bios.2018.04.002

Omnexus. (2017). *Polyethylene terephthalate (PET): A comprehensive review*. PET Plastic (Polyethylene Terephthalate): Uses, Properties & Structure. Retrieved from https://omnexus.specialchem.com/selection-guide/polyethylene-terephthalate-pet-plastic

Pandey, C. M., Augustine, S., Kumar, S., Kumar, S., Nara, S., Srivastava, S., & Malhotra, B. D. (2017). Microfluidics based point-of-care diagnostics. *Biotechnology Journal, 13*(1), 1700047. https://doi.org/10.1002/biot.201700047

Prost, S., Kishen, R. E., Kluth, D. C., & Bellamy, C. O. (2016). Working with commercially available quantum dots for immunofluorescence on tissue sections. *PLOS ONE, 11*(9). https://doi.org/10.1371/journal.pone.0163856

Ramachandran, N., Hainsworth, E., Bhullar, B., Eisenstein, S., Rosen, B., Lau, A. Y., Walter, J. C., & LaBaer, J. (2004). Self-assembling protein microarrays. *Science, 305*(5680), 86–90. https://doi.org/10.1126/science.1097639

Reuschenbach, M., Waterboer, T., Wallin, K.-L., Einenkel, J., Dillner, J., Hamsikova, E., Eschenbach, D., Zimmer, H., Heilig, B., Kopitz, J., Pawlita, M., Doeberitz, M. von, & Wentzensen, N. (2008). Characterization of humoral immune responses against

P16, p53, HPV16 E6 and HPV16 E7 in patients with HPV-associated cancers. *International Journal of Cancer*, *123*(11), 2626–2631. https://doi.org/10.1002/ijc.23837

Rusling, J. F., Kumar, C. V., Gutkind, J. S., & Patel, V. (2010). Measurement of biomarker proteins for point-of-care early detection and monitoring of cancer. *The Analyst*, *135*(10), 2496. https://doi.org/10.1039/c0an00204f

Rositch, A. F., Gatuguta, A., Choi, R. Y., Guthrie, B. L., Mackelprang, R. D., Bosire, R., Manyara, L., Kiarie, J. N., Smith, J. S., & Farquhar, C. (2012). Knowledge and Acceptability of Pap Smears, Self-Sampling and HPV Vaccination among Adult Women in Kenya. *PLOS ONE*, *7*(7), e40766. https://doi.org/10.1371/journal.pone.0040766

Sankaranarayanan, R., Nene, B. M., Shastri, S. S., Jayant, K., Muwonge, R., Budukh, A. M., Hingmire, S., Malvi, S. G., Thorat, R., Kothari, A., Chinoy, R., Kelkar, R., Kane, S., Desai, S., Keskar, V. R., Rajeshwarkar, R., Panse, N., & Dinshaw, K. A. (2009). HPV Screening for Cervical Cancer in Rural India. *New England Journal of Medicine*, *360*(14), 1385–1394. https://doi.org/10.1056/NEJMoa0808516

Smola, S. (2017). Immunopathogenesis of HPV-Associated Cancers and Prospects for Immunotherapy. *Viruses*, *9*(9), 254. https://doi.org/10.3390/v9090254

Sonker, M., Sahore, V., & Woolley, A. T. (2017). Recent advances in microfluidic sample preparation and separation techniques for Molecular Biomarker Analysis: A critical review. *Analytica Chimica Acta*, *986*, 1–11. https://doi.org/10.1016/j.aca.2017.07.043

Sorger, P. K. (2008). Microfluidics closes in on point-of-care assays. *Nature Biotechnology*, *26*(12), 1345–1346. https://doi.org/10.1038/nbt1208-1345

Stanley, M. (2010). Hpv - immune response to infection and vaccination. *Infectious Agents and Cancer*, *5*(1). https://doi.org/10.1186/1750-9378-5-19

Starcevic Manning, M., Kroenke, M. A., Lee, S. A., Harrison, S. E., Hoofring, S. A., Mytych, D. T., & Jawa, V. (2017). Assay signal as an alternative to titer for assessment of magnitude of an antidrug antibody response. *Bioanalysis*, *9*(23), 1849–1858. https://doi.org/10.4155/bio-2017-0185

Thermo Fisher Scientific. (2013). Dynabeads® MyOne™ Carboxylic Acid: Product Manual. Retrieved from https://www.thermofisher.com/document-connect/document-connect.html?url=https%3A%2F%2Fassets.thermofisher.com%2FTFS-Assets%2FLSG%2Fmanuals%2F65011_65012_Dynabeads_MyOne_Carboxylic_Acid_PI.pdf

Thermo Fisher Scientific. (2015a). *Alexa Fluor 488 dye: Thermo Fisher Scientific - US*. Alexa Fluor 488 dye | Thermo Fisher Scientific - US. Retrieved March 2, 2022, from https://www.thermofisher.com/us/en/home/life-science/cell-analysis/fluorophores/alexa-fluor-488.html

Thermo Fisher Scientific. (2015b). *Physical Properties of Dynabeads Magnetic Beads*. Dynabeads Nucleic Acid Purification Support—Getting Started. Retrieved from https://www.thermofisher.com/us/en/home/technical-resources/technical-reference-library/nucleic-acid-purification-analysis-support-center/dynabeads-nucleic-acid-purification-support/dynabeads-nucleic-acid-purification-support-getting-started.html

Thermo Fisher Scientific. (2017). Thermo Scientific Immunoassay Plate Guide: User Guide. Retrieved from http://assets.thermofisher.com/TFS-Assets/LCD/Scientific-Resources/Immunoassay_Plate_Guide.pdf

Tsai, H. Y., Wu, H. H., Chou, B. C., Li, C. S., Gau, B. Z., Lin, Z. Y., & Fuh, C. B. (2019). A magneto-microfluidic platform for fluorescence immunosensing using quantum dot nanoparticles. *Nanotechnology*, *30*(50), 505101. https://doi.org/10.1088/1361-6528/ab423d

Vashist, S. K., & Luong, J. H. (2018). Chapter 4 - Bioanalytical Requirements and Regulatory Guidelines for Immunoassays. In *Handbook of Immunoassay Technologies: Approaches, performances, and applications* (pp. 81–95). Academic Press.

Van Dyne, E. A., Henley, S. J., Saraiya, M., Thomas, C. C., Markowitz, L. E., & Benard, V. B. (2018). Trends in Human Papillomavirus–Associated Cancers—United States, 1999–2015. *Morbidity and Mortality Weekly Report*, *67*(33), 918–924. https://doi.org/10.15585/mmwr.mm6733a2

Vinodhini, K., Shanmughapriya, S., Sanmugham, S., Senthikumar, G., Das, B. C., & Natarajaseenivasan, K. (2012). Prevalence of high-risk HPV and associated risk factors in cases of cervical carcinoma in Tamil Nadu, India. *International Journal of Gynecology & Obstetrics*, *119*(3), 253–256. https://doi.org/10.1016/j.ijgo.2012.06.019

Zhao, Z., Yang, Y., Zeng, Y., & He, M. (2016). A microfluidic ExoSearch chip for multiplexed exosome detection towards blood-based ovarian cancer diagnosis. *Lab on a Chip*, *16*(3), 489–496. https://doi.org/10.1039/c5lc01117e

Zare, R. N. (2017). Making materials that hate water to love water: The transformative power of chemistry. *Molecular Frontiers Journal*, *01*(01), 10–15. https://doi.org/10.1142/s2529732517400028

Zhang, Y. (2015). *The Hook Effect. Pearls of Laboratory Medicine: The Hook Effect* . American Association for Clinical Chemistry. Retrieved from https://www.aacc.org/science-and-research/clinical-chemistry-trainee-council/trainee-council-in-english/pearls-of-laboratory-medicine/2014/the-hook-effect

Zhu, M., Obahiagbon, U., Anderson, K. S., & Christen, J. B. (2017). Highly sensitive fluorescence-based lateral flow platform for point-of-care detection of biomarkers in plasma. *2017 IEEE Healthcare Innovations and Point of Care Technologies (HI-POCT)*. https://doi.org/10.1109/hic.2017.8227631